NAVAL POSTGRADUATE SCHOOL

MONTEREY, CALIFORNIA

THESIS

PHYSICAL AND OPTICAL PROPERTIES OF ATMOSPHERIC AEROSOLS MEASURED FROM A COASTAL SITE

by

Eric R. Dridge

June 2017

Thesis Advisor: Haflidi Jonsson
Co-Advisor: Qing Wang

Approved for public release. Distribution is unlimited.

THIS PAGE INTENTIONALLY LEFT BLANK

REPORT DOCUMENTATION PAGE			Form Approved OMB No. 0704-0188

1. AGENCY USE ONLY *(Leave blank)*	2. REPORT DATE	3. REPORT TYPE AND DATES COVERED
	June 2017	Master's thesis

4. TITLE AND SUBTITLE
PHYSICAL AND OPTICAL PROPERTIES OF ATMOSPHERIC AEROSOLS MEASURED FROM A COASTAL SITE

5. FUNDING NUMBERS

6. AUTHOR(S) Eric R. Dridge

7. PERFORMING ORGANIZATION NAME(S) AND ADDRESS(ES)
Naval Postgraduate School
Monterey, CA 93943-5000

8. PERFORMING ORGANIZATION REPORT NUMBER

9. SPONSORING /MONITORING AGENCY NAME(S) AND ADDRESS(ES)
N/A

10. SPONSORING / MONITORING AGENCY REPORT NUMBER

11. SUPPLEMENTARY NOTES The views expressed in this thesis are those of the author and do not reflect the official policy or position of the Department of Defense or the U.S. Government. IRB number ____N/A____.

12a. DISTRIBUTION / AVAILABILITY STATEMENT
Approved for public release. Distribution is unlimited.

12b. DISTRIBUTION CODE

13. ABSTRACT (maximum 200 words)

Improving the United States' electromagnetic (EM) and electro-optical (EO) prediction capabilities is imperative to maintaining a tactical advantage in the operational environment. The objective of this research is to estimate aerosol effects on radiative transfer through the atmosphere, particularly the contribution due to coastal surf-generated aerosol, and will include the characterization and measurement of marine aerosols, especially in coastal regions. This research involves analysis of the aerosol data, specifically the total extinction coefficient, collected during CASPER (Coupled Air Sea Processes and Electromagnetic Ducting Research)-East from various sensors deployed off the coast of Duck, North Carolina, from 9 October 2015 to 6 November 2015. Sea, land, and along-shore breeze periods were closely examined and compared by particle concentration, size and volume distribution, and through extinction coefficients. These data were then examined for possible correlation with wind speed and direction. In sustained along-shore wind periods with an active surf zone, a large impact is observed on the optical effects of the aerosol. A strong transport barrier associated with sharp sea surface temperature gradients was observed in unstable air during cold advection of land- and surf-contaminated aerosol.

14. SUBJECT TERMS	15. NUMBER OF PAGES
CASPER, coastal aerosol, optical effects	69
	16. PRICE CODE

17. SECURITY CLASSIFICATION OF REPORT	18. SECURITY CLASSIFICATION OF THIS PAGE	19. SECURITY CLASSIFICATION OF ABSTRACT	20. LIMITATION OF ABSTRACT
Unclassified	Unclassified	Unclassified	UU

NSN 7540-01-280-5500 Standard Form 298 (Rev. 2-89)
Prescribed by ANSI Std. 239-18

THIS PAGE INTENTIONALLY LEFT BLANK

Approved for public release. Distribution is unlimited.

PHYSICAL AND OPTICAL PROPERTIES OF ATMOSPHERIC AEROSOLS MEASURED FROM A COASTAL SITE

Eric R. Dridge
Lieutenant, United States Navy
B.S., United States Naval Academy, 2006

Submitted in partial fulfillment of the
requirements for the degree of

MASTER OF SCIENCE IN METEOROLOGY AND PHYSICAL OCEANOGRAPHY

from the

NAVAL POSTGRADUATE SCHOOL
June 2017

Approved by: Haflidi Jonsson
Thesis Advisor

Qing Wang
Co-Advisor

Wendell Nuss
Chair, Department of Meteorology

THIS PAGE INTENTIONALLY LEFT BLANK

ABSTRACT

Improving the United States' electromagnetic (EM) and electro-optical (EO) prediction capabilities is imperative to maintaining a tactical advantage in the operational environment. The objective of this research is to estimate aerosol effects on radiative transfer through the atmosphere, particularly the contribution due to coastal surf-generated aerosol, and will include the characterization and measurement of marine aerosols, especially in coastal regions. This research involves analysis of the aerosol data, specifically the total extinction coefficient, collected during CASPER (Coupled Air Sea Processes and Electromagnetic Ducting Research)-East from various sensors deployed off the coast of Duck, North Carolina, from 9 October 2015 to 6 November 2015. Sea, land, and along-shore breeze periods were closely examined and compared by particle concentration, size and volume distribution, and through extinction coefficients. These data were then examined for possible correlation with wind speed and direction. In sustained along-shore wind periods with an active surf zone, a large impact is observed on the optical effects of the aerosol. A strong transport barrier associated with sharp sea surface temperature gradients was observed in unstable air during cold advection of land- and surf-contaminated aerosol.

THIS PAGE INTENTIONALLY LEFT BLANK

TABLE OF CONTENTS

LIST OF FIGURES

LIST OF ACRONYMS AND ABBREVIATIONS

AC	aircraft
β_{ap}	absorption coefficient
CASPER	Coupled Air-Sea Processes and Electromagnetic Ducting Research
CIRPAS	Center for Interdisciplinary Remotely-Piloted Aircraft Studies
CPC	TSI 310 Condensation Particle Counter
D_p	particle diameter
EM	electromagnetic
EMW	Electromagnetic Maneuver Warfare
EO	electro-optical
FLIR	forward looking infrared
FRF	Field Research Facility
GARP	GEMPAK Analysis and Rendering Program
MABL	marine atmospheric boundary layer
NASU	NPS Aerosol Sampling Unit
NEPH	TSI Integrating 3563 Nephelometer
PCASP	Passive Cavity Aerosol Spectrometer Probe
PSAP	Three-Wavelength Particle Soot Absorption Photometer
RF	radio frequency
R/V	research vessel
SST	sea surface temperature
TS	total scatter
UTC	Coordinated Universal Time

THIS PAGE INTENTIONALLY LEFT BLANK

I. INTRODUCTION

A. THESIS OBJECTIVES

Improving the United States' electromagnetic (EM) and electro-optical (EO) prediction capabilities is imperative to maintaining a tactical advantage in the operational environment. The objective of this research is to estimate aerosol effects on radiative transfer through the atmosphere, particularly the contribution due to coastal surf-generated aerosol, and will include the characterization and measurement of marine aerosols, especially in coastal regions. To estimate aerosol effects on radiative transfer through the atmosphere, the physical and optical properties of the surf-generated aerosol will be obtained over the surf zone and background aerosol characteristics will be obtained over the ocean away from the surf zone. These datasets will be independently analyzed and compared to reveal the role of the breaking waves in the surf zone in generating additional aerosols and their potential impact on EM/EO propagation.

Aerosol generation from the ocean can occur from a variety of different processes and is greatly increased when winds increase and white caps occur, but there is a lack of aerosol data adequate for model evaluation and/or improvement. This research involves analysis of the aerosol data, specifically absorption, and total scatter coefficients, which constitute the total extinction coefficient, collected during CASPER (Coupled Air Sea Processes and Electromagnetic Ducting Research)-East from 9 October 2015 to 6 November 2015.

The data were collected from various sensors deployed off the coast of Duck, North Carolina, to obtain environmental properties, and concurrent air-sea interaction and radio frequency propagation sampling. These platforms were designed to address sea and atmospheric surface layer characteristics, and their effects on EM propagation. This involved measurements of aerosols, sea surface temperature (SST), surface wave variability, coastal thermal circulation/SST front circulation, and internal boundary layer development. The CASPER-East dataset to be analyzed includes aerosol particle concentrations, absorption and scattering coefficients, and particle size distributions.

Since one of the most pressing issues for EM/EO Propagation Prediction is the lack of data adequate for model evaluation or improvement, this quality-controlled dataset collected during CASPER-East will help fill the void. This thesis work attempts to quantify surf zone-generated aerosols with persistent measurements over a period of one month.

B. IMPORTANCE OF STUDY

The marine boundary layers, especially near the coastal regions, are characteristically heterogeneous and often transient. This is especially true for aerosol concentration, which is inherently difficult to quantify and predict with only a limited amount of information collected in selected regions. As will be discussed in Chapter II, the aerosol concentration in the surf zone is probably the least well characterized due to the persistent wave breaking and the combination of land and ocean influences. Yet, aerosol scattering and absorption are the key factors affecting optical imaging, target detection, and high energy laser (HEL) system performances. In addition, the thermodynamics of sea spray generation and the subsequent evaporation of sea spray droplets can indirectly affect EM propagation in the microwave range by influencing temperature and humidity profiles near the surface. The purpose of CASPER is to address overarching knowledge gaps related to EM wave propagation in the coastal marine atmospheric boundary layer (MABL). The objective is to "fully characterize the MABL as an EM propagation environment" with "emphasis … on spatial and temporal heterogeneities and surface wave/swell effects" (Wang et al. 2015).

The proposed research will advance our knowledge of the coastal aerosols associated with surf zone and their impacts on EM/EO propagation in the marine boundary layer. It will also provide a much-needed dataset that can be used to improve and tune aerosol and visibility prediction models to forecast targeting and detection ranges. Future developments in improving propagation prediction depend on understanding the atmosphere and upper ocean interactions, and correctly quantifying the characteristics of the surface layer environment. This successfully completes a portion of

the CASPER objective to obtain data adequate for EM model evaluation and improvement.

C. U.S. NAVAL APPLICATION

U.S. Naval platforms and sensors rely on the most advanced technologies to operate above, below, and at the air-sea interface to support current operations. It is important to understand environmental characteristics and how they affect platforms, personnel, and equipment during military operations. U.S. Naval platforms and sensors depend heavily on EM propagation for communications and data transfer, as well as detection and targeting, with an "increasing use of weapons, intelligence and surveillance systems operating at visible, infrared and microwave frequencies" which "places greater dependence on information relating to the radiative and physical characteristics of the lower atmosphere" (Edson et al. 1999). Chief of Naval Operations Admiral Greenert stated that "the EM spectrum ... is essential to our military operations. Failing to use it effectively will be the difference between victory and defeat" (Stewart 2014).

Small changes in the environmental characteristics, such as temperature and humidity, have a large effect on EM propagation, including communications, and electromagnetic wave detection (radar). When the conditions are right, strong surface-based ducts can propagate electronic signals well beyond system designed ranges. This can lead to increased detection ranges, but also may increase the surface clutter and reduce system performance. Small changes in sea spray aerosol content can indirectly affect EM propagation, by influencing temperature and humidity, or directly attenuate EO signals. Increased aerosol content in the lower boundary layer can decrease the probability of detection of small ships or low flying aircraft and missiles. System performance degradation can also occur due to increased EO mirages or scintillation. It is important to understand the environmental characteristics that the U.S. Navy operates in to increase accuracy of model predictions, improve system performance and operator knowledge, and ensure vulnerabilities of various platforms and equipment are understood.

Rear Admiral Gallaudet, Commander Naval Meteorology and Oceanography Command, stresses the importance of understanding the operational environment and by maintaining awareness of the surroundings and that "Naval Oceanography provides the home-field advantage to the fleet's away games" (Naval Meteorology and Oceanography Command Public Affairs 2016). Rear Admiral Gallaudet recently released his commands Electromagnetic Maneuver Warfare (EMW) Strategy on March 9, 2017. The goals of the EMW Strategy are: "1) Influence development of the Navy's electromagnetic maneuver warfare capabilities. 2) Improve Naval Oceanography's environmental sensing and prediction capabilities. 3) Integrate electromagnetic environmental impacts into the Navy's decision-making process" (Gallaudet 2016). This thesis addresses Rear Admiral Gallaudet's first two goals and will help improve the U.S. Navy's environmental prediction capabilities and EMW capabilities.

II. BACKGROUND

A. COUPLED AIR-SEA PROCESSES AND ELECTROMAGNETIC DUCTING RESEARCH (CASPER)

CASPER is a multi-disciplinary university research initiative sponsored by the Office of Naval Research (ONR) to address overarching knowledge gaps related to EM wave propagation in the MABL (Wang et al. 2017). One element of CASPER is the field program, which focuses on characterizing various ducting conditions by concurrent measurements of the atmosphere, ocean, and EM propagation. The other element of CASPER is numerical modeling, which involves a multi-scale modeling approach with close interaction between observations and modeling efforts (Wang et al. 2017).

The field program has two main campaigns: CASPER-East and CASPER-West. CASPER-East took place in Duck, North Carolina, from 9 October 2015 to 6 November 2015, and the "focus … was on assessing the effects of heterogeneous marine environment on EM propagation and on the uncertainties introduced to evaporation duct modeling" (Wang et al. 2017). CASPER-West is planned to take place at Point Mugu, California, in the fall of 2017, with the objective to "evaluate wave/swell effects on evaporation duct properties and various modeling issues associated with elevated trapping layers" (Wang et al. 2017). This thesis is centered on the field program, specifically analyzing data obtained from CASPER-East at and around the pier operated by the U.S. Army Corps of Engineers at their Field Research Facility (FRF) at Duck, North Carolina.

B. SEA AEROSOL GENERATION

Sea salt aerosol generation from the ocean largely depends on the strength of the winds. According to Lewis (2004), winds of 5 ms^{-1} or greater at 10 meters are strong enough to move the water at the surface faster than the water below the surface, thus generating waves. When waves break, air is entrained to various depths, which creates bubbles that rise to the surface and burst, trapping sea water and ejecting sea salt aerosols in the atmosphere. When these bubbles burst two types of spray droplets, film droplets

and jet droplets, are formed. Film droplets are produced when bubbles burst at the surface of the ocean, generating several hundred (Twomey 1977), tiny (1–30 micrometers) film droplets per bubble (Resch 1986) as the bubble surface disintegrates. Jet droplets are produced when the internal cavity of the bubble collapses and the liquid on the bubble walls is ejected into the atmosphere, causing a vertical jet to be produced. 1–10 jet droplets are produced per bubble at 0.1–0.15 times the size of the bubble (Resch 1986). When droplets are ejected from the surface and evaporate, the residual sea salt remains in the atmosphere. At the same time, the evaporation affects both the temperature and humidity of the air.

Another formation mechanism of sea salt aerosols occurs with winds of at least 7–11 ms^{-1} (Spiel and Leeuw 1996), with sufficient energy to cause mechanical disruption of the waves and rip water droplets off the wave crests. This formation mechanism produces droplets known as spume droplets which are projected nearly horizontally and are larger than film and jet droplets. Spume drops are typically 20 micrometers or larger (Edson et al. 1999).

When some of the film, jet, or spume droplets, or raindrops, fall back and strike the sea surface, more droplets are produced, and these droplets are known as splash droplets. Splash droplets are around 100 micrometers but "fall out" of the atmosphere "quickly and do not usually travel very far from their source" (Twomey 1977). "Generally, the spume droplets account for most of the spray volume flux while splash droplets are generally believed to be an insignificant part of the total spray volume" (Edson et al. 1999).

Sea salt aerosol particles mix with the marine atmosphere and greatly impact the background particle concentration and size distributions that affect EM/EO properties. The sea salt aerosols directly affect EO properties by intercepting and redistributing beams, and indirectly affect EM propagation through temperature and humidity gradients to directly affect the surface based duct size and strength. "Over the oceans, sufficiently far away from continents, the sea aerosol concentrations range from 100 to 200 particles per cubic centimeter and are fairly constant" (Fenn 1976). Clean maritime air concentrations are generally 1,500 particles/cc (Hess et al. 1998). Sea spray aerosol is

typically larger than background, land-sourced aerosol. “Sea spray aerosol … concentration begins to decrease for particles less than 0.2 micrometers” (Fenn 1976). “The vertical distribution of aerosol particles in the atmosphere has been found to decrease very rapidly with increasing altitude for the first four to five kilometers” (Fenn 1976). Meteoric dust and volcanic dust particles contribute to the particle concentration at high altitudes (Fenn 1976). Even with all this information, it is impossible to determine the exact contribution of sea salt particles to overall aerosol extinction in the atmosphere without chemical characterization of the particle composition.

C. LAND AEROSOL GENERATION

Continental aerosol generation can occur from nucleation in supersaturated gasses emitted from combustion, natural emission from vegetation, lofting of surface dust, or by “splintering from solid or liquid surfaces, such as rocks, road surfaces or machinery,” as described by Twomey (1977). Dusts, fumes, smoke, smog, and haze are all forms of land aerosols. Dusts are formed by disintegration, such as through mining activities. “Fumes usually result from chemical reactions, such as oxidation” in exhaust plumes, and are typically in the “0.01 to less than one micrometer” range (Dennis 1976), but increase in size with time due to collisions and coagulation. Smokes, which can result from combustion of fossil fuels, are “associated with obscuring optics” and are approximately 0.5 micrometers (Dennis 1976). Smog and haze are broad atmospheric terms and contain “submicron particles or droplets produced by chemical reactions or condensation processes in the atmosphere” (Dennis 1976). These land aerosols are transported by winds across the world and are mixed with sea sourced particles. Continental air generally has a higher particle concentration than marine air and can range from 2,600 particles/cc in clean continental air particle concentration and increase to over 50,000 particles/cc when polluted (Hess et al. 1998).

D. EXTINCTION COEFFICIENT

The data collected during CASPER-East will be analyzed to determine the aerosol characteristics, specifically absorption, and total scattering coefficients, which combine into a total extinction coefficient. The extinction coefficient (σ), also known as

attenuation coefficient, characterizes how a beam of radiation attenuates as it transmits through a medium, and is measured in inverse length units. Attenuation can be caused by one of the two processes (absorption, scattering) or any combination of the two (University Corporation for Atmospheric Research [UCAR] 2014). The extinction coefficient is the sum of the absorption coefficient (σ_a), and scattering coefficient (σ_s), as shown in Equation (1).

$$\sigma = \sigma_a + \sigma_s \tag{1}$$

An aerosol photometer measures the absorption coefficient, while a nephelometer measures the total scattering coefficient. A particle counter measures aerosol particle concentration, and a passive cavity aerosol spectrometer measures the particle size distribution.

Scattering is caused by small particles suspended in the atmosphere that diffuse a portion of the incident radiation in all directions. Scattering changes the spatial distribution of the energy without transforming the energy, and thus decreases the energy in the direct beam. "Because of the small wavelengths in the visible portion of the EO spectrum (0.4 to 0.74 microns), scattering is worst for the visible wavelength" (Naval Meteorology and Oceanography Professional Development Detachment Atlantic 2005).

Absorption is caused by small particles suspended in the atmosphere that retain the incident radiant energy (warm up), and is an irreversible transformation of radiation into another energy form. Absorption is caused by particles containing, or are entirely composed of, black carbon, but at some wavelengths absorption is also caused by water vapor, carbon dioxide and ozone, and to smaller extent by other gases. Typically, the aerosol absorption coefficient is much smaller than the scattering coefficient in the MABL. "Absorption is VERY SIGNIFICANT with FLIR sensors and is the most significant cause of infrared contrast degradation" (Naval Meteorology and Oceanography Professional Development Detachment Atlantic 2005).

Brightness (B) is defined as the intensity of radiant energy per unit area normal to the direction of light propagation. Once the extinction coefficient (σ) is known, Beer's Law can be used to solve for optical attenuation and changes to the brightness with

distance. In Equation (2), (x) is the distance from the source, and B_o is the intensity at the source.

$$B = B_o e^{-\sigma x} \tag{2}$$

Transmissivity of the air (τ) is defined as the ratio of transmitted radiation to the total incident radiation, as shown in Equation (3). Transmission is the process for the propagation of the incident radiation through a medium.

$$\tau = \frac{B}{B_o} \tag{3}$$

Once the conditions of the environment are determined, a visual range can be calculated. "During the day, visibility is measured using Koschmieder's Law," (Bennett 2012) as shown in Equation (4). The meteorological range (V), is based off the atmospheric extinction coefficient (σ) and the threshold contrast (C_T). The threshold contrast is set to 0.05, which was determined as a "realistic minimum contrast identifiable to an observer" (Bennett 2012).

$$V = \frac{-\ln(C_T)}{\sigma} \tag{4}$$

THIS PAGE INTENTIONALLY LEFT BLANK

III. EXPERIMENTAL DATA

A. EXPERIMENTAL SETUP

The data were collected from various sensors deployed off the coast of Duck, North Carolina, at the pier operated by the U.S. Army Corp of Engineers at their Field Research Facility (FRF), shown in Figure 1. Several research platforms were used to obtain concurrent air-sea interaction and RF propagation sampling. Major platforms included: CIRPAS Twin Otter, R/V *Atlantic Explorer*, R/V *Hugh R. Sharp*, Wave Gliders, wave buoys, flux buoys and a shore site.

The NPS Aerosol Sampling Unit (NASU) is a multi-sensor instrument package that includes a TSI Integrating 3563 Nephelometer (NEPH), a Three-Wavelength Particle Soot Absorption Photometer (PSAP), and a TSI 310 Condensation Particle Counter (CPC) in a self-contained sampling container approximately 1.5 meters tall, 1.2 meters wide, and 1 meter in depth. The NASU also includes a "weather" sensor package to measure temperature, humidity, and mean wind.

The NEPH measures total scatter signals at three wavelengths (450, 550 and 700 nm) by "measuring the light scattered by aerosol particles" (TSI Incorporated 2012), while the PSAP allows for a "continuous measurement of absorption by monitoring the change in transmittance across a filter" (Bond et al. 1999). The CPC measures the concentration of particles in the nanometer to micrometer range by using a host alcohol, to grow the particles to a detectable size, and an optical counter that counts them individually in a constant rate flow (TSI Incorporated 2006).

NASU was deployed on the FRF pier during CASPER-East between 7 October 2015 and 6 November 2015. An aerial view of the FRF pier is shown in Figure 1, with the location of the NASU indicated by the arrow. A picture of the NASU deployed on the pier during CASPER-East is shown in Figure 2. The deck of the pier is 7.7 meters above mean sea level, varying with tides. The opening of the aerosol inlet is about three meters from the deck, which corresponds to approximately 10.3 meters above mean sea level.

The inlet was topped by a metal sheet to minimize intrusion of rain water into the sampling system.

Figure 1. U.S. Army Corps of Engineers Field Research Facility, Duck, North Carolina.

Figure 2. NASU Deployed on the FRF Pier.

The data from the NEPH and PSAP were quality controlled and corrected for total scattering and absorption errors. From this pier data, absorption and total scatter coefficients as well as an extinction coefficient were calculated. The data were then analyzed for various lengths of duration (the entire experiment period, daily variation, and variations on time scale of hours) to determine variations associated with changes in general weather conditions.

The CIRPAS Twin Otter operated on 11 days during the experiment and flew along preplanned tracks. One of the instruments onboard was the Passive Cavity Aerosol Spectrometer Probe (PCASP), which measured aerosol particle size distributions by "measuring the intensity of the light that the particle scatters when passing through a light beam" (Baumgardner 2005). Another PCASP was also deployed on the pier.

B. SYNOPTIC EVENTS

Duck, North Carolina, is a coastal town with a barrier island environment that consists of a narrow strip of land separating the Atlantic Ocean to the east from the Currituck Sound to the west. Winds are typically geostrophic in the area, flowing from west to east at 4–5 ms^{-1}, but are affected by any storms that pass by the area. Synoptic snapshots from GARP are shown in Figures 3, 4, and 5, where the red cursor highlights the location of Duck, North Carolina. A typical synoptic snapshot of the area when not influenced by storms or high pressure systems is shown in Figure 3.

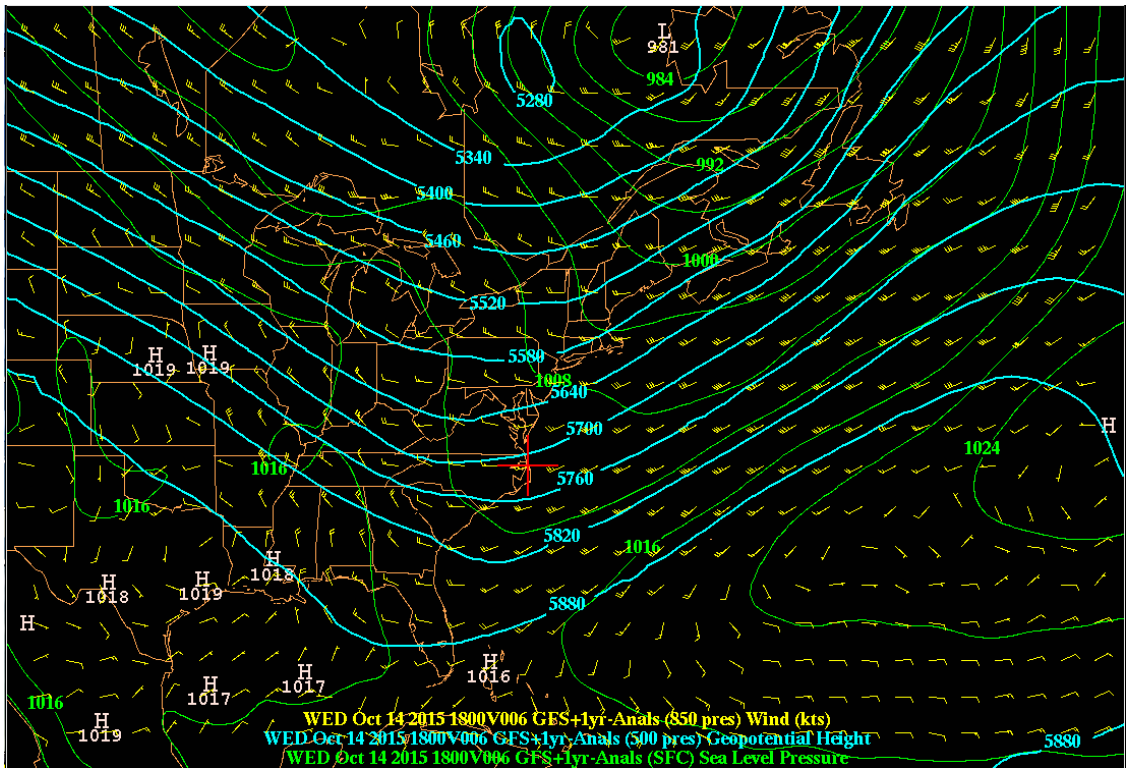

The Red '+' Sign Indicates the Location of Duck, NC.

Figure 3. Synoptic Scale Conditions from GFS Forecast on 14 October 2015.

Storm systems influenced the area on 16, 19, and 28 through 29 October 2015 and 1 November 2015, and varied the wind direction from off-shore to on-shore and increased wind speeds up to 20 ms^{-1} at Duck, North Carolina. The storm on 29 October 2015 is highlighted in Figure 4. This mid-latitude cyclone developed in the Gulf of Mexico on 28 October 2015 and strengthened and propagated northeastward through the Midwest to the Northeast by 30 October 2015. The winds shifted from westerly to southerly and increased in speed to 18 ms^{-1}.

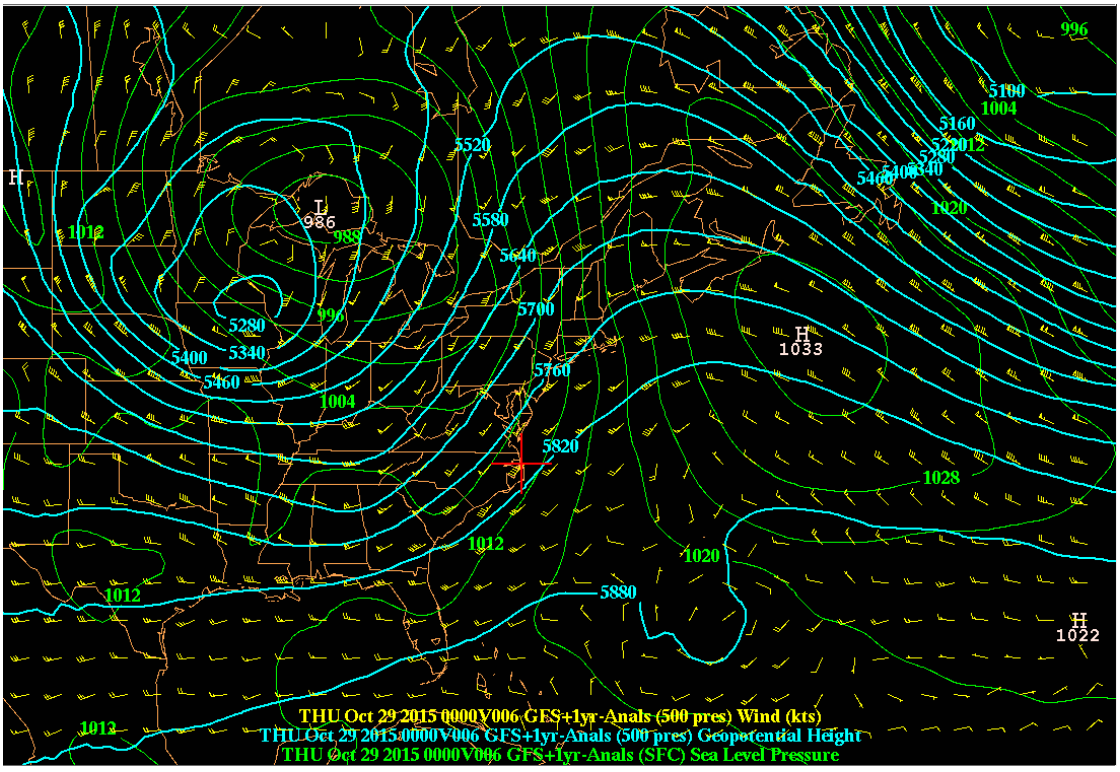

The Red '+' Sign Indicates the Location of Duck, NC.

Figure 4. Synoptic Scale Conditions from GFS Forecast on 29 October 2015.

A high pressure system dominates the experimental area from 19 October through 27 October 2015 and 1 through 4 November 2015. This high pressure system blocks any synoptic storm events and winds are typically light and variable. 20 October 2015 is representative of the synoptic picture during most of the aircraft flights and is shown in Figure 5.

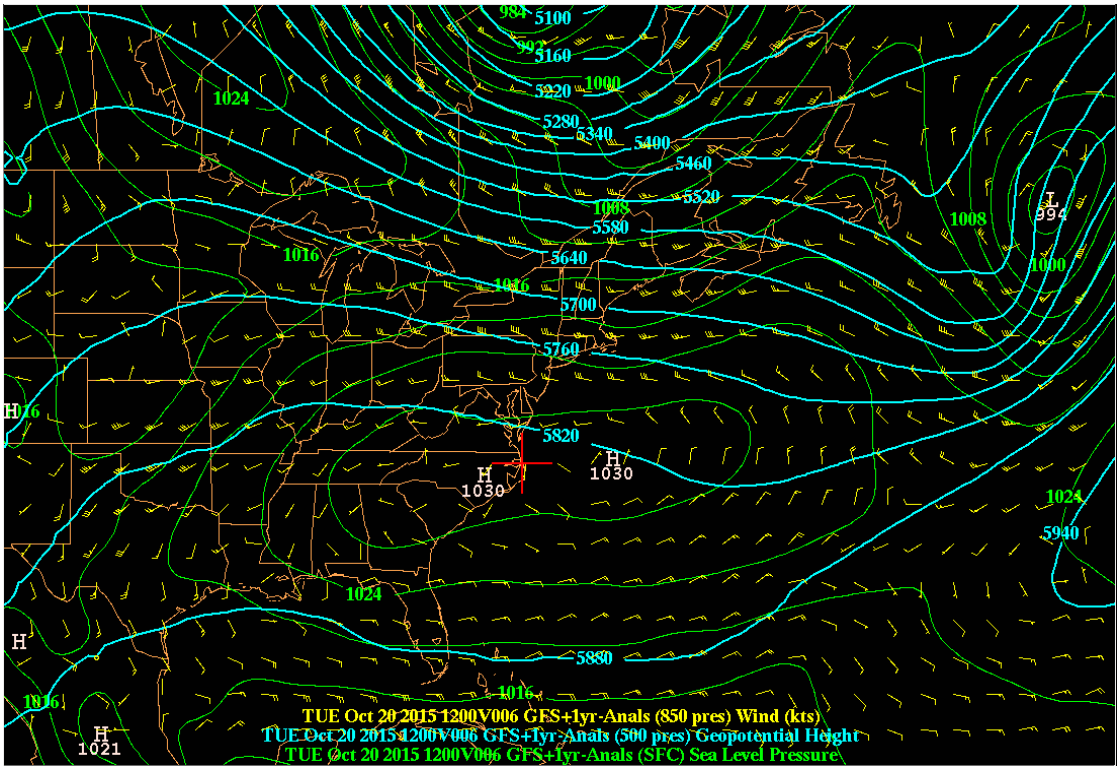

The Red '+' Sign Indicates the Location of Duck, NC.

Figure 5. Synoptic Scale Conditions from GFS Forecast on 20 October 2015.

This thesis closely examines measured data on 17 October 2015 and the weather patterns for this day are provided in Figures 6 and 7. The following is an in-depth synoptic analysis for 17 October 2015. In-depth daily analysis for the entirety of CASPER can be found in Hale et al. (2016).

> Sustained moderate offshore flow dominates the CASPER region as a strong 1034mb surface high pressure over Illinois and strong northwesterly flow aloft are both pushing dry, near record cold, polar air southeast from Canada to the eastern United States. The nighttime overcast clears out near shore as the surface front moves further offshore, but clouds do linger much of day as cold advection strato-cumulus forms over the Gulf Stream. A surface high pressure ridges offshore to the north and shifts southward, as a final shortwave and dry cold front sweep in

from the northwest in the evening. Surface winds back from NNE 15knots in the morning to NW 10 knots in the afternoon as the front approaches and maintains a northerly choppy 3–5 ft seas. The air advection out over CASPER has dried and cooled further to about 17C and 2C dewpoint which is becoming increasingly unstable over the warmer water and stratocumulus lingers over and south of the Gulf Stream. (Hale et al. 2016)

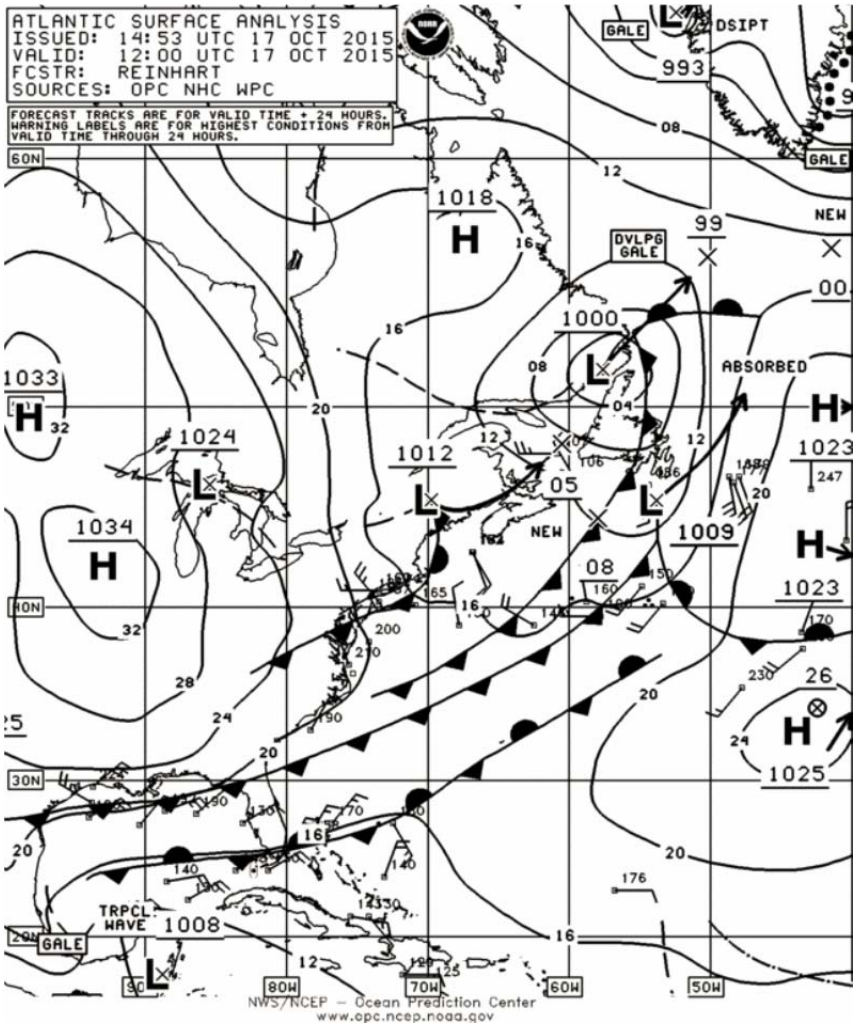

Figure 6. Surface Pressure and Frontal Synoptic Systems on 17 October 2015. Source: Hale et al. (2016).

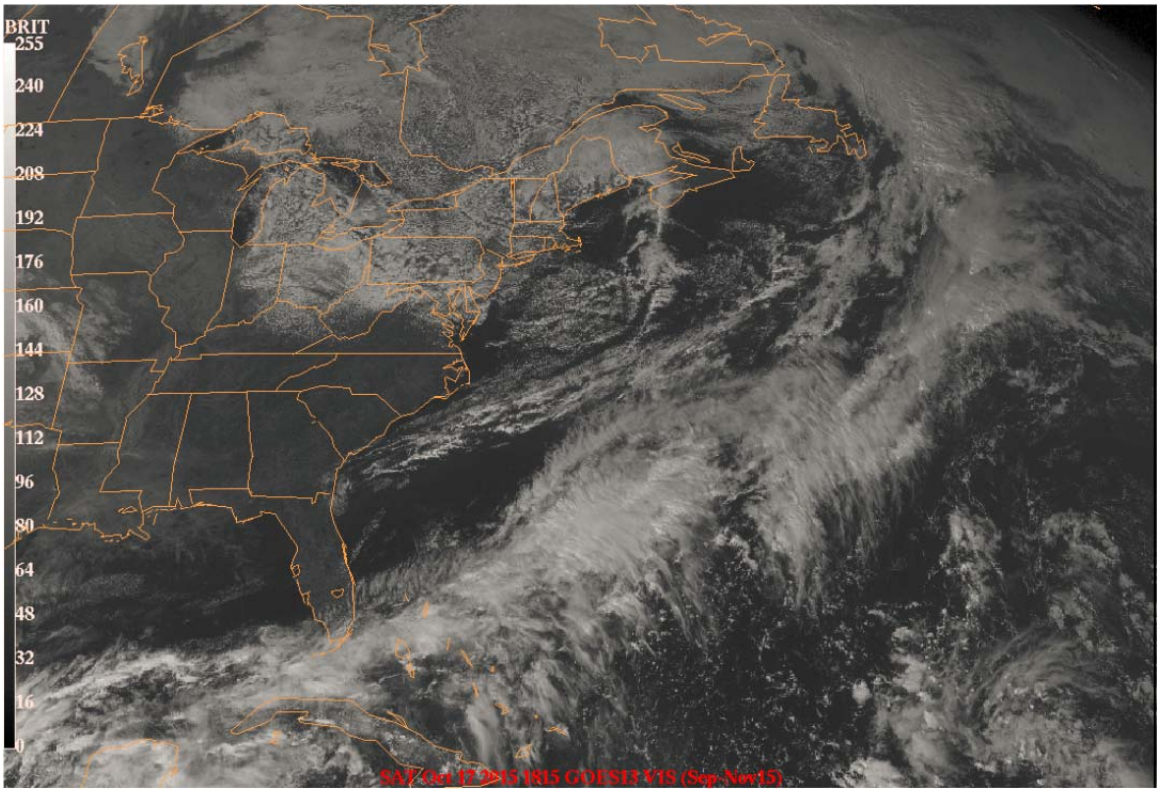

Figure 7. GOES13 Visible Satellite on 17 October 2015.
Source: Hale et al. (2016).

C. INSTRUMENTS

The NASU was deployed on the FRF pier for the entirety of CASPER-East and contained a NEPH, PSAP and CPC, as well as a "weather" sensor package. A PCASP was deployed on the pier for a portion of CASPER-East and another PCASP and "weather" sensor package were deployed on the CIRPAS Twin Otter during flight operations. These instruments provide the data to be examined that allows for the aerosol effects on radiative transfer through the atmosphere to be estimated. Operational descriptions of each instrument are provided in the following subsections.

1. TSI Integrating 3563 Nephelometer (NEPH)

The NEPH measures light scattering properties of atmospheric aerosols, such as total scatter, by continuously drawing air through the inlet and into the sensing volume and by "measuring the light scattered by aerosol particles and subtracting light scattered

by the gas" (TSI Incorporated 2012). The "sample is illuminated over an angle of 7–170 degrees by a halogen light source" and "viewed by three photomultiplier tubes" (TSI Incorporated 2012) as shown in Figure 8. The dark backdrop of the sensing volume and an efficient light trap in the NEPH are designed to reduce scattering contributions from the walls. The NEPH is affected by all sizes of particles, as continuous measurements of light are scattered by the sample aerosol.

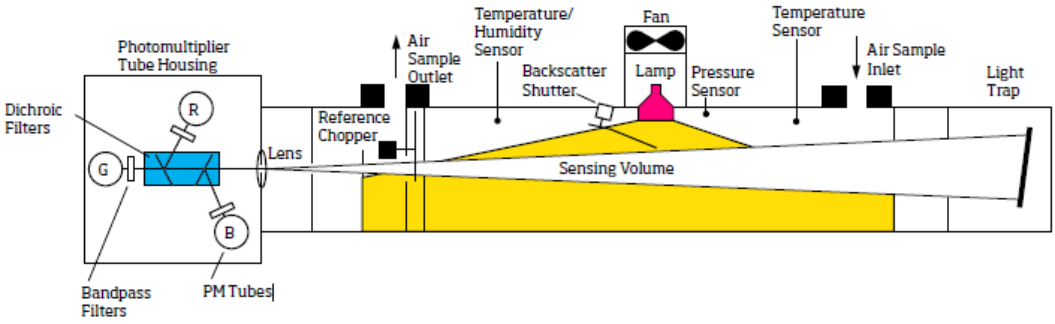

Figure 8. NEPH. Source: TSI Incorporated (2012).

2. Three-Wavelength Particle Soot Absorption Photometer (PSAP)

The PSAP measures absorption by continuously drawing sample air through a sampling hole that allows particles to deposit on the filter (Bond et al. 1999). Filtered air is drawn through another other hole as a reference measurement, as shown in Figure 9. The calculation of the absorption coefficient is based on the measured change in light intensity for a given amount of air drawn through the filter by use of Equation (5), where "A is the area of the sample spot, V is the volume of air drawn through the spot area during a given time period", and τ are the "filter transmittances before and after the time period" (Virkkula et al. 2005).

$$\sigma = \frac{A}{V} \ln[\frac{\tau_0}{\tau}] \quad (5)$$

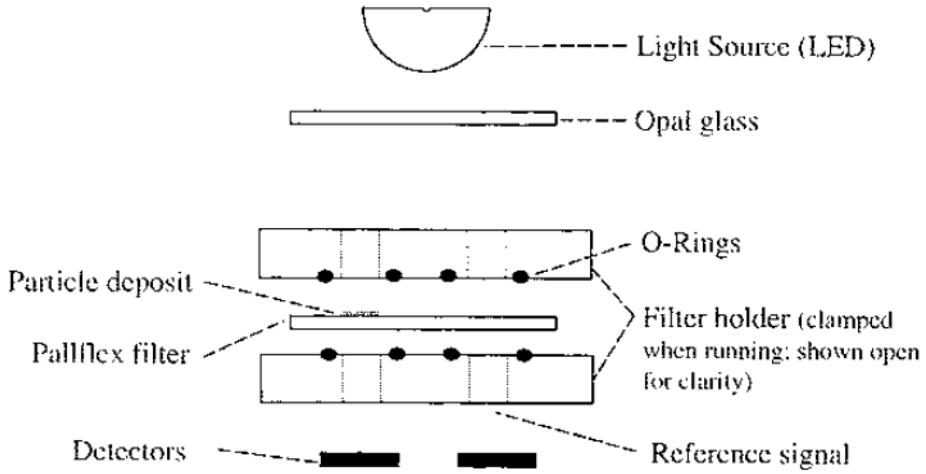

Figure 9. PSAP. Source: Bond et al. (1999).

3. Passive Cavity Aerosol Spectrometer Probe (PCASP)

PCASP measures particle size by "measuring the intensity of the light that the particle scatters when passing through a light beam" (Baumgardner 2005). The optical path of the instrument is shown in Figure 10. A "helium-neon laser beam is focused to a small diameter at the center of an aerodynamically focused particle laden air stream" (Baumgardner 2005). This beam is scattered by individual particles that the beam comes in contact with and some of this scattered "light is collected by a mangin mirror" (Baumgardner 2005). The collected light is measured by a photodetector and categorized into one of 20 size bins. "The size of the particle is determined by measuring the light scattering intensity and using Mie scattering theory to relate this intensity to particle size" (Baumgardner 2005). PCASP is designed for particles 100 nm to three microns but the calibration of the pier PCASP showed that detection threshold was 143 nm, while the aircraft PCASP detection threshold was 100 nm. Pulse heights measured by these instruments are grouped into 20 bins based on measured pulse heights, which subsequently are converted to diameter on bases of calibration.

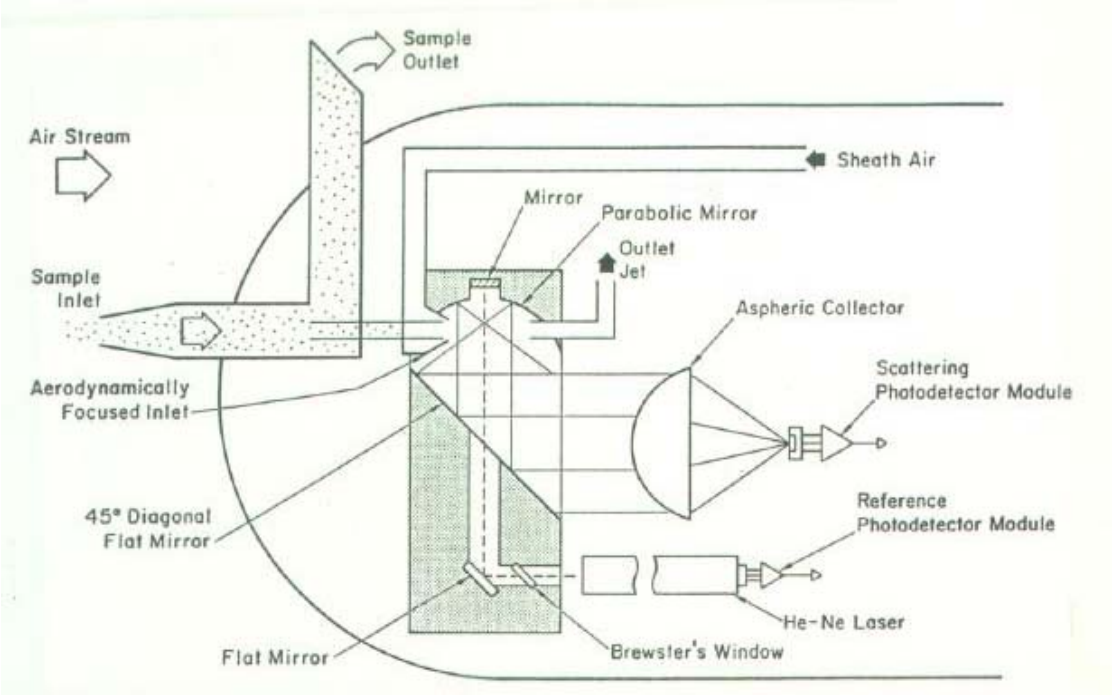

Figure 10. PCASP. Source: Baumgardner (2005).

4. TSI 310 Condensation Particle Counter (CPC)

The NASU on the FRF pier also contained a Condensation Particle Counter (CPC). An external vacuum pump is used to draw aerosol samples through the CPC. Alcohol is heated until vaporization occurs and then diffused into the aerosol sample stream. "Alcohol condenses onto particles in the sample flow, creating aerosol droplets large enough to be detected efficiently using a light-scattering technique" (TSI Incorporated 2006). Each aerosol droplet is counted as an individual pulse as the droplets pass through the sensing zone. An operational diagram of the CPC is shown in Figure 11. The CPC detects airborne particles from 10 nm to several microns in diameter (TSI Incorporated 2006) and are measured in number of counts per cc (#/cc). The aerosol flow through the counter is controlled at a constant rate by a critical orifice to allow determination of particle concentration.

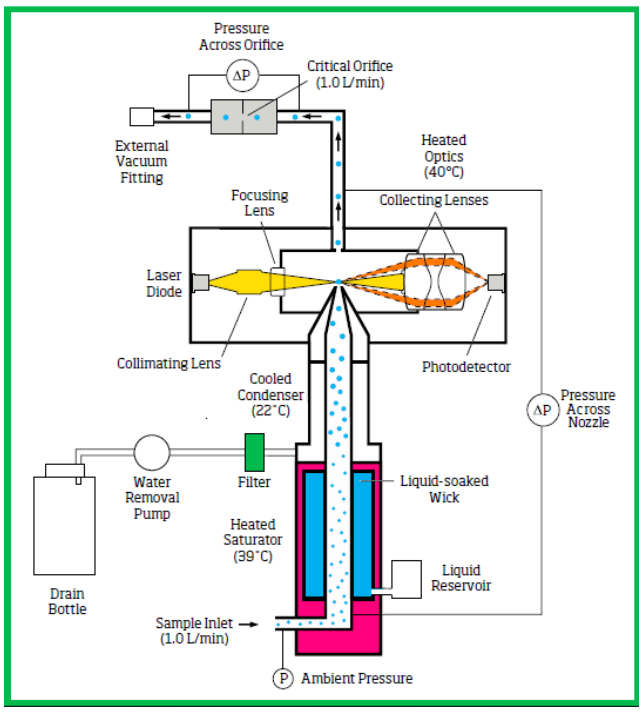

Figure 11. CPC. Source: TSI Incorporated (2006).

IV. DATA PROCESSING AND RESULTS

A. DATA QUALITY CONTROL

Extensive quality control was performed on the NEPH, PSAP, CPC and PCASP datasets. This includes identifying and applying correction factors to the NEPH and PSAP, converting PCASP size distributions to scattering coefficients, and removal of erroneous data in the original dataset. This section will outline these efforts.

1. NEPH Correction

"Two factors contribute to biasing NEPH sensitivity away from near-forward scattering: Truncation error (the geometrical blockage of near-forward-scattered light for angles below 7 deg) and nonlambertian error (the slightly noncosine-weighted intensity distribution of illumination light provided by the opal glass diffuser)" (Anderson and Ogren 1998). Anderson and Ogren (1998) monitored NEPH responses and created a "diagnostic record of instrument performance" which was used to "improve instrument accuracy". Correction factors for total scatter as a linear function of Angstrom exponent, as shown in Equation (6), are provided by the paper of Anderson and Ogren (1998), where C is the correction factor, a and b are constants, and $\dot{A}$ is the Angstrom exponent.

$$C = a + b * \dot{A} \tag{6}$$

From the NEPH data, Angstrom coefficients (blue, green, red) were determined from measured total scatter (TS), as shown in Equation (7), where λ represents wavelength, and subscript 1 and 2 denote the two wavelengths and associated TS being examined. Angstrom coefficients describe the dependence of aerosol optical thickness on wavelength and are a convenient, qualitative, descriptor of aerosol particle size.

$$\dot{A}(\frac{\lambda_1}{\lambda_2}) = -\log(\frac{TS_1}{TS_2}) / \log(\lambda_1 \diagup \lambda_2) \tag{7}$$

Anderson and Ogren (1998) noted that "NEPH measurements of TS ... contain systematic errors due to angular and wavelength nonidealities" and a correction factor must be determined, provided by Equation (8).

$$C = \frac{TS_{True}}{TS_{NEPH}} \tag{8}$$

These correction factors were applied to the measured TS values from NEPH, as shown in Equation (9) where C is taken from Equation (6)

$$TS_{corrected} = TS_{NEPH} * C \tag{9}$$

2. PSAP Correction

PSAP calibration corrections were given by Bond et al. (1999) as "several factors can lead to overestimation of absorption by filter-based measurement methods." The instrument's flow rate and spot size assumptions were verified for this instrument, thus flow and spot size corrections were determined to be unnecessary. Corrections were needed for instrument precision (ε_{slope} and ε_{noise}), which are calculated from Equation (10) and Equation (11), where $\sigma_{ap,measured}$ is the measured absorption coefficient from PSAP (Bond et al. 1999), τ_0 is the initial transmittance, and τ is the final transmittance.

$$\varepsilon_{slope}(\mu m) = 0.06\sigma_{ap,measured} \tag{10}$$

$$\varepsilon_{noise}(\mu m) = 0.18\sqrt{\tau_0 / \tau} \tag{11}$$

Corrections were also needed for PSAP response to scattering aerosol (K_1) and PSAP response to absorption (K_2), which is calculated through Equation (12), where σ_{adj} is the reported value after the flow and spot size corrections, and σ_{sp} is the scattering coefficient at 550 nm (Bond et al. 1999).

$$\sigma_{ap} = \frac{\sigma_{adj} - K_1\sigma_{sp} + \varepsilon_{slope} + \varepsilon_{noise}}{K_2} \tag{12}$$

Measured absorption cross-section was adjusted for flow rate and spot size corrections and then corrected due to the other factors. The PSAP's intake is the NEPH's outflow to assure that both instruments measured the same sample. The NEPH sampling is non-destructive, so there is no sampling correction needed.

3. PCASP Conversion to Scattering

Mie scatter theory was used to calculate scattering cross sections for the optically active particle sizes measured by the PCASP. This was done for the wavelengths of the NEPH and PSAP and the relevant refractive index. Oceanic spectral refractive indices for scatter (real) and absorption (imaginary) (1.50+0*i) were used for 400, 550, 700 nm (blue, green, red) wavelengths (Levoni et al. 1997). The absorption coefficient was assumed to be zero in these calculations as the measurements show that the absorption coefficient was generally an order of magnitude smaller than the scattering coefficient. Scattering cross sections were calculated for the geometric mean diameter of each PCASP size bin and multiplied by particle counts to give total scatter. Since the PCASP does not detect particles smaller than 100 nm or larger than about two microns, these calculated extinction coefficients are expected to be smaller than those obtained from the NEPH and PSAP, which only are limited by possible particle losses in the sample transport system.

4. Erroneous Data Removal

The dataset was thoroughly examined and erroneous data were removed, such as when instruments were secured or running a self-check. Every three hours the NEPH required a "zeroing" technique to reset the baseline. The air intake flow was filtered to allow the NEPH to measure the scattering due solely to air molecules and the felt covering the measuring chamber and any particles that were trapped on it. This "zeroing" affected the PSAP and CPC as well, since their intakes were attached to the NEPH outlet flow. These zeroing procedures appeared in the dataset as clearly identifiable anomalies, and were subsequently removed during quality control. The PSAP needed to be secured periodically to replace the filter. These erroneous data points were removed. The PCASP was secured from 9–10 October 2015 and from 21 October until the end of CASPER-East. The CPC was secured from 28 October until the end of CASPER-East.

B. OVERALL RESULTS

An aerial view of the experimental site with separations of major wind sectors is shown in Figure 12. The coastline running north from the pier corresponds to 0^o from the North and the coastline to the south corresponds to 180^o, while the pier corresponds to relative 90^o wind direction. The land breeze is defined as sustained winds from 190^o to 350^o and will be shaded in following figures in red. A sea breeze is defined as sustained winds from 010–170^o and will be shaded in following figures in blue. Winds from 350–010^o and 170–190^o are defined as coastal winds and may contain land and sea generated aerosols and will be left unshaded.

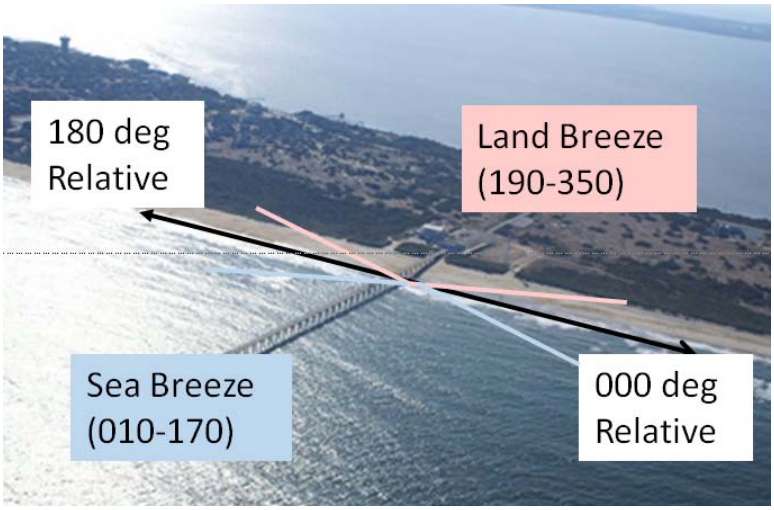

Figure 12. Aerial View of the Experimental Site with Breeze Annotations.

An overview of the pier data from 7 October 2015 to 28 October 2015 is shown in Figure 13. A log-scale of the total scatter coefficient measurement in inverse megameter is shown in the first subplot; the log-scale of the absorption coefficient (β_{ap}) in inverse megameter is shown in the second subplot; the CPC in counts per cubic centimeter is shown in the third subplot; the wind speed in meters per second is shown in the fourth subplot. The experimental setup was occasionally tampered with if small craft traversed in the vicinity of the pier instrument's sample intake. This increased flux of exhaust

fumes falsely increased the natural particle concentration that was not caused by normal sea salt or land aerosols.

Also, there were a few times of precipitation, which can be seen in the NEPH data as large spikes, usually ahead of transition from land breeze to sea breeze, or vice versa. Raindrops are typically 0.5 to 4 mm, and splash off the intake top hat. Thus, water fragments may make their way into the sampling system during rain events and could affect the NEPH measurements.

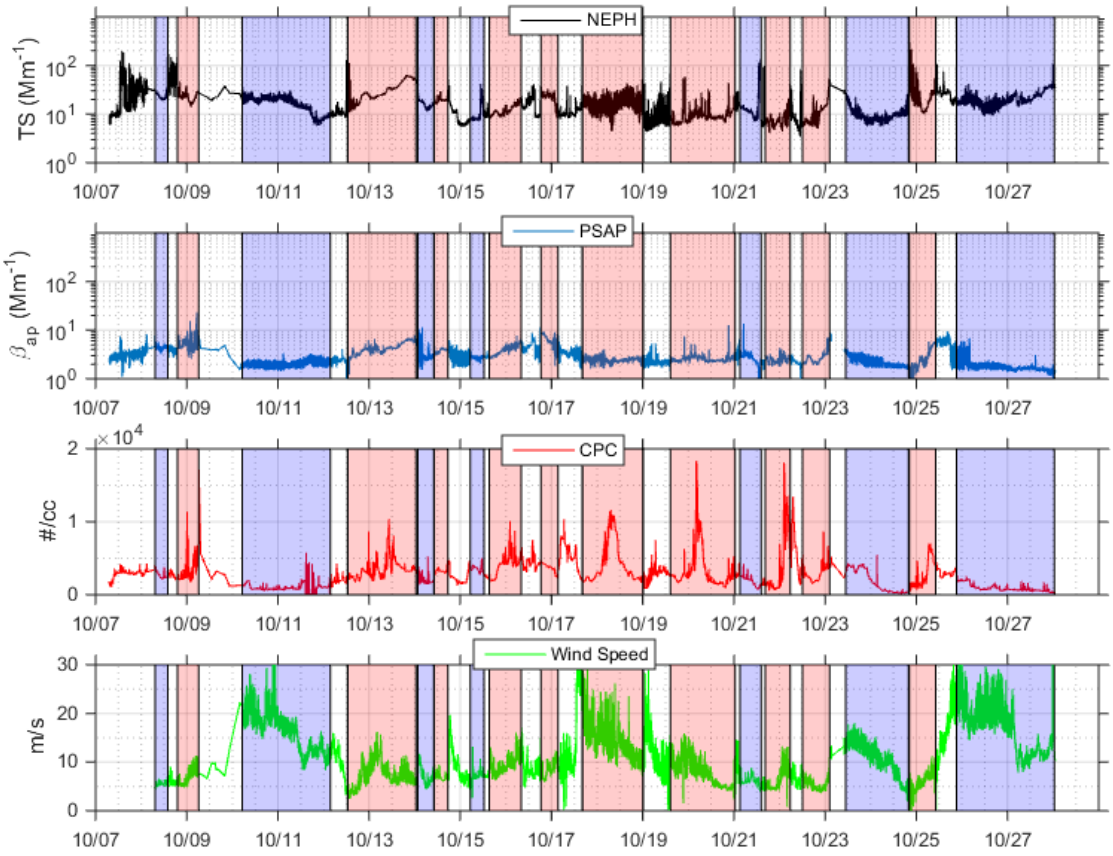

Red shading on the plots indicates land breeze while the blue shading indicates sea breeze. Unshaded sections indicate either light and variable winds or coastal-parallel winds.

Figure 13. An Overview of Pier-Based Wind and Aerosol Measurements for the Entire CASPER-East Period.

Large fluctuations, by more than two orders of magnitude, over the period are observed in Figure 13. The minima, particularly in particle concentration and absorption, appear coincidental with periods of sea breezes, while the maxima seem associated with the continental air. As indicated in the background section, sea salt aerosols are generally larger and fewer than the land-sourced aerosols and some (the largest ones) may not be detected by the CPC. The large sea salt particles are generally very few, and while they contribute greatly to scattering, they contribute little to the CPC counts. There are large spikes in CPC counts when the winds shift to a land breeze. The absorption coefficient is also typically at a minimum during sea breeze periods. The total scatter measured by the NEPH has a more complicated pattern, with less clear relationship to wind direction overall, although in some land breeze periods total scatter steadily rises until the wind direction transitions.

A comparison of the NEPH measured total scatter (TS) for the green wavelength (550 nm) and the PCASP calculated TS green (550 nm) wavelength is shown in Figure 14. The PCASP calculated TS values are lower than the NEPH values throughout the experiment, due to the PCASP technical capabilities that can only detect aerosols from around 143 nm to three microns. The NEPH measures scattering from any aerosol or particle that flows into the measuring chamber and thus is affected by both smaller and larger particles than the PCASP can measure. PCASP scatter is thus expected to be smaller in general than the scatter measured by the NEPH. PCASP measurements stop on 20 October 2015 when the instrument was secured.

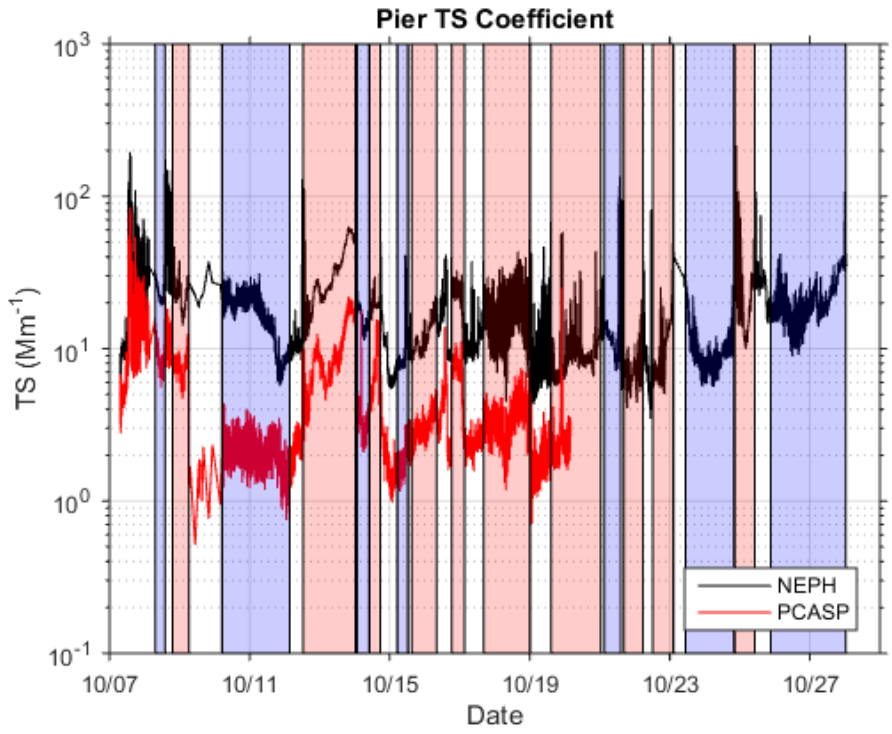

Red shading on the plot indicates land breeze while the blue shading indicates sea breeze. Unshaded sections indicate either light and variable winds or coastal-parallel winds. All measurements were made from the FRF pier.

Figure 14. A Comparison of Total Scatter Measured by the NEPH and Calculated Based on PCASP Aerosol Size Distribution.

From Figure 14, on 13, 16, and 18 October 2015, the TS coefficient increases steadily during the land breeze periods. The largest values of TS occur during the end of the land breeze periods, right before the wind direction switches to coastal or sea breeze. During the one lengthy sea breeze period on 11 October 2015, the TS decreases when measured by the NEPH and PCASP. The general trends of the measured TS from the NEPH and the calculated TS from PCASP are consistent. This provides a confidence in the sampling of both instruments.

Pseudocolor (pcolor) plots were used to examine the size distributions for the entire dataset. A pcolor plot that showcases the size distributions for each 60 second average of time is shown in Figure 15. On most days, there is a peak in size distribution around 0.2 microns in diameter. There are a few instances where another peak appears near 0.4 microns, which occurs from 7–9, 13–15, and on 17 October 2015. From 7–8

October 2015, occasionally the size distribution broadens to approximately a one micron diameter. On the first day of measurements (7 October 2015), the size distribution spreads to two microns. Wind speed is overlaid on the psuedoplot to provide a sense of the environmental conditions. Unfortunately, the wind speed measurement was not initiated until 8 October 2015. A storm occurred on 7 October 2015 with wind speeds up to 20 ms^{-1} from the northeast, which coated the area with spray and sea salt. In subsequent high wind speed conditions (approximately 30 ms^{-1}), the size distribution is predominately around 0.2 microns, but when the wind speed decreases, the size distribution broadens to larger sizes. Often, the maximum spread in the size distribution coincides with relatively low wind speeds. Wind direction shading is shown at the top of Figure 15, with red shading indicating land breeze periods and blue shading indicating sea breeze periods.

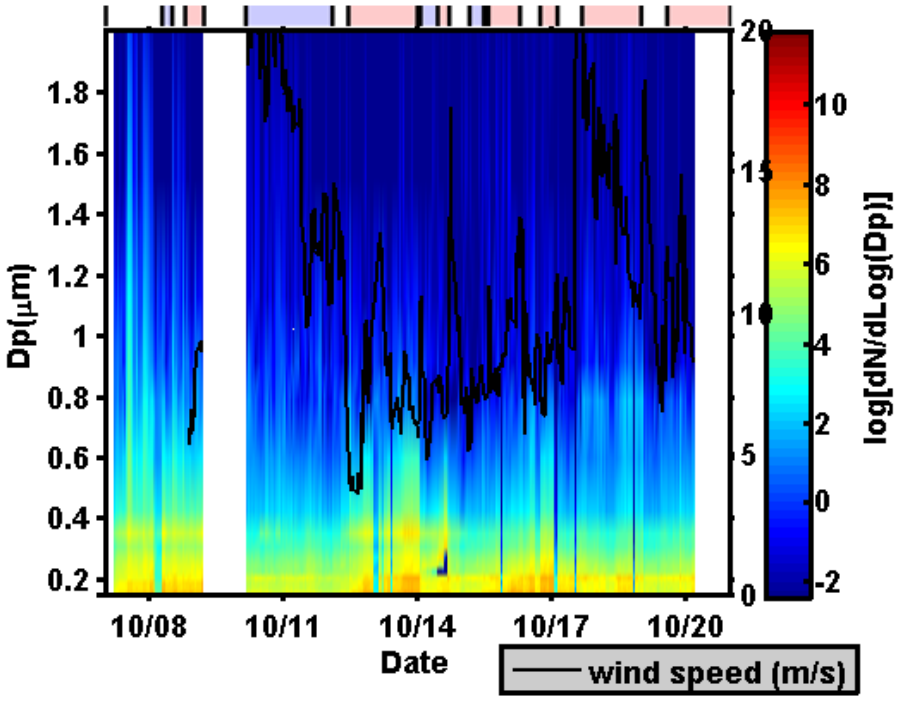

Red shading on the top of the plot indicates land breeze while the blue shading indicates sea breeze. Unshaded sections indicate either light and variable winds or coastal-parallel winds. Wind speed is shown on the right y-axis.

Figure 15. PCASP Size Distribution.

Aerosol extinction relates to a higher order of the particle size and is therefore more sensitive to larger size particles. The size distribution hence does not illustrate the aerosol effect very well. To better illustrate the aerosol effects, the size distributions were converted to a volume distribution (third order of size) shown in Figure 16 over the period of PCASP measurements. Large variations in the volume distribution are seen. Occasionally the broadening of the volume distribution coincides with high wind speeds, but the correlation is poor. Wind direction shading is shown at the top of Figure 16, with red shading indicating land breeze periods and blue shading indicating sea breeze periods.

The volume concentrations in Figure 16 show a broad range of distribution for both the land and sea breeze periods, indicating the presence of large sized particles associated with sea salt aerosols. This may be due to the geographical conditions at Duck, North Carolina. A large body of water is not only on the Atlantic side of the site, but also a short distance to the west. Thus, surf generation of particles is possible in both land and sea breezes.

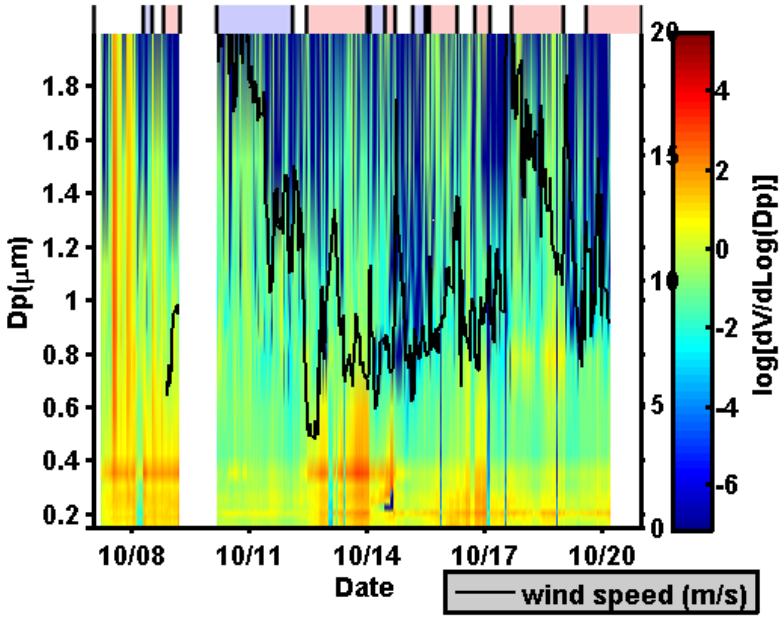

Red shading on the top of the plot indicates land breeze while the blue shading indicates sea breeze. Unshaded sections indicate either light and variable winds or coastal-parallel winds. Wind speed is shown on the right y-axis.

Figure 16. PCASP Volume Distribution.

C. SURF GENERATION OF PARTICLES

As mentioned before, the CPC measures concentration of particles in approximately three nanometers to one micron diameter size range. To further examine the CPC counts, the data were separated into land breeze and sea breeze conditions based on sustained wind direction. The land breeze and sea breeze datasets were then compared to wind speed for analysis (Figures 17 and 18). In Figures 17 and 18, each diamond represents an average over a period of 60 seconds of winds from either 010–170^{o} (sea breeze) or 190–350^{o} (land breeze).

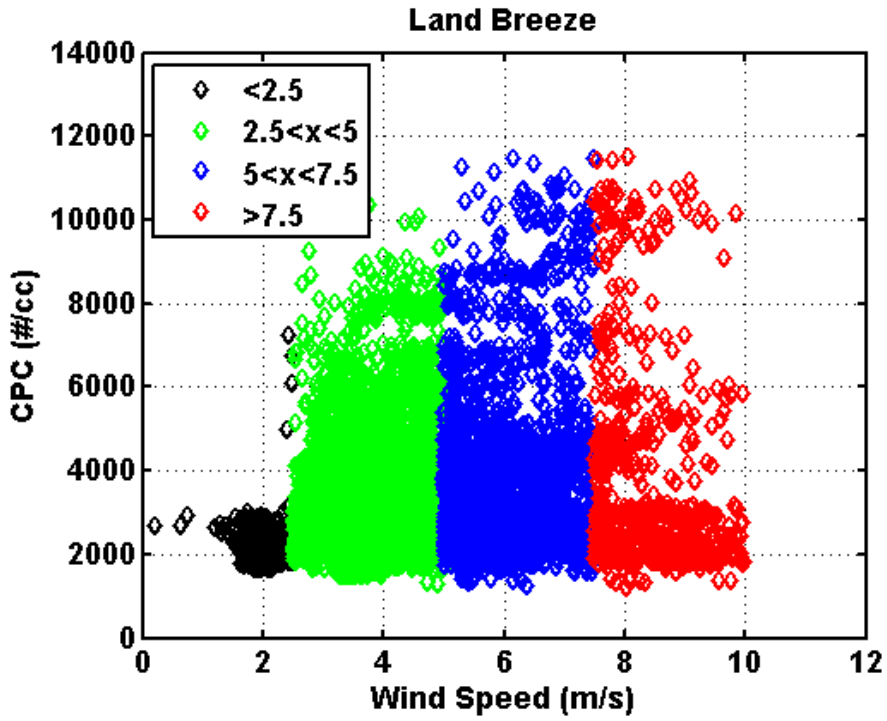

Figure 17. CPC Counts during Periods of Land Breeze.

The land breeze, which is typically comprised of small particles formed by gas to particle formation in plumes and mixed into the atmosphere, has a maximum of nearly 12,000 counts per cubic centimeter (cc). The land breeze has a minimum of 1,500 #/cc that occurs at all wind speeds. When the land breeze is less than 2.5 ms^{-1}, the particle concentration is relatively steady, and relatively low, possibly a reflection of few local sources in the vicinity of the pier. As the winds increase to greater than 2.5 ms^{-1}, the

dispersion in the particle count increases dramatically, as particles from distant sources (cities, highways, power plants, etc.) are blown to the coast.

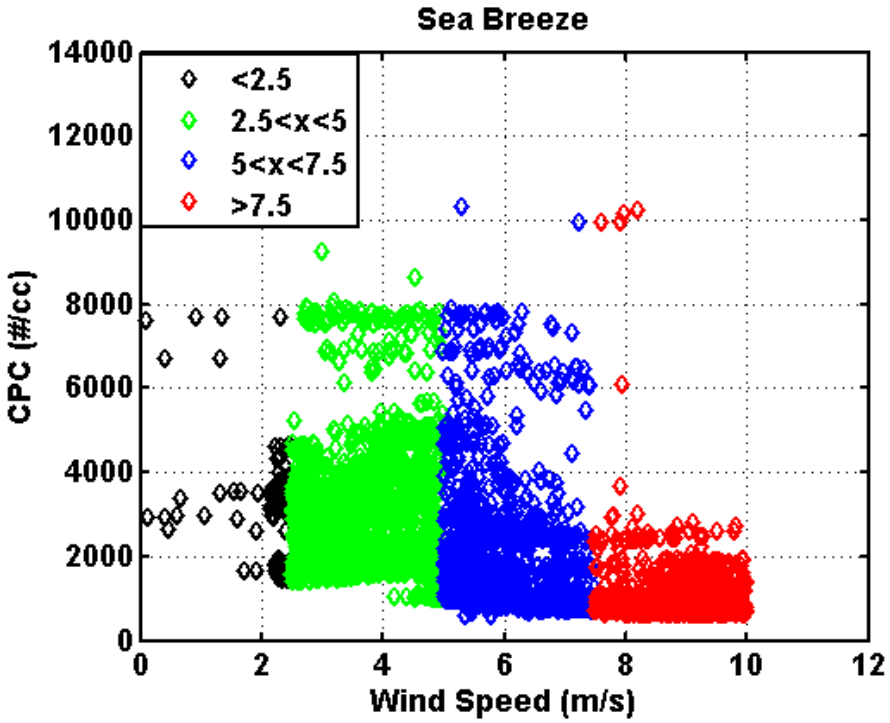

Figure 18. CPC Counts during Periods of Sea Breeze.

In the sea breeze the trend of variation in CPC count as a function of wind speed is similar to that during land breeze, but generally shows a lower maximum particle concentration and less occurrence of events of high particle counts. The sea breeze maximum number concentration in sea breeze conditions is about 8,000 #/cc, which is less than the measured maximum particle concentration during periods of land breeze. The sea generated aerosol is made up of mostly sea salt particles, with scarce sources of sulfates formed by nucleation over the oceans or in exhaust plumes from shipping. Although, during preceding land breeze periods, continental aerosol is carried out to sea, and is brought back to shore when the winds shift. This possible land aerosol contamination can be seen in wind speeds less than 8 ms^{-1}. When wind speeds are over 8 ms^{-1}, particle concentrations are relatively low, suggesting that only at high wind speeds does pure marine aerosol reach the coast. Otherwise, due to the frequent shifts in wind

direction, land-sourced aerosols that was advected over the water surface may be advected back towards the shore.

D. OFFSHORE/ONSHORE TRANSITION PERIODS

An in-depth view of a period where the wind shifts from land breeze (red shading), through the coast line (unshaded) and becomes sea breeze (blue shading) is shown in Figure 19. The TS from the NEPH, as well as CPC counts, Angstrom coefficient, and wind speed are shown. The CPC has higher particle concentration for the land breeze than the sea breeze, but the highest counts occur during sustained winds along the coastline, where the wind has had a long fetch over the surf zone. This sustained coastline breeze period seems sufficient to create a buildup of surf generated sea salt particles, reaching a near steady state concentration at the pier. In the sea breeze period, the fetch is limited to the width of the surf zone.

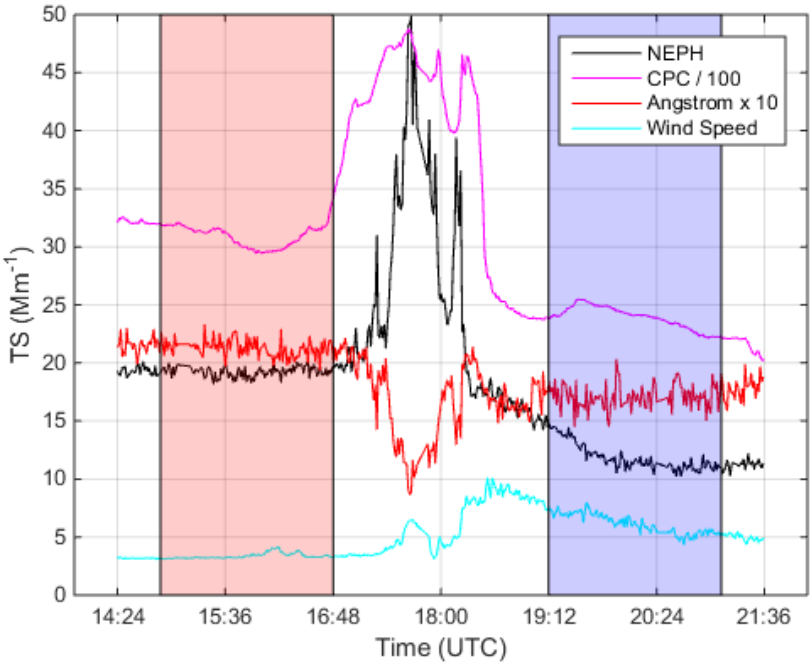

Red shading on the plot indicates land breeze while the blue shading indicates sea breeze. Unshaded sections indicate either light and variable winds or coastal-parallel winds.

Figure 19. Pier-Based Aerosol and Scattering/Extinction Measurements in Periods of Different Wind Directions on 14 October 2015.

During the period of coastline breeze favorable for surf-generated aerosols, the TS from the NEPH has dramatically increased from both the land breeze situation and the subsequent sea breeze situation. This coincides with an increase in CPC counts. During the sea breeze period, NEPH TS and CPC counts are at a minimum, although wind speed was comparably high and reaches ~10 ms^{-1} during a short period. This wind speed increase would indicate possible whitecaps, which may have led to an increase in large sea surf aerosols. NEPH TS and CPC counts decrease as the wind turns from along the coastline to onshore later in the day.

There is a dramatic drop in value of the Angstrom coefficient during the along-shore period, indicating a shift in the particle size distribution toward larger particles when the scattering coefficient peaks. During the next time period with onshore flow, the Angstrom coefficient recovers as scatter decreases, indicating a shift back to smaller particles; however, it remains lower than during the off-shore breeze, indicating a proportionally larger effect on TS by large particles in the marine air than in the land-sourced air. At the same time, the scattering coefficient is larger and CPC counts are higher in the land breeze than in the sea breeze.

The NEPH TS was converted to visual range using Equation (4), and is shown in Figure 20.

The size distributions from PCASP on the pier are shown in Figure 21. These measurements were made concurrently with the data shown in Figure 20. The land breeze around 16:00 (UTC) is depicted by *land*, the coastline breeze around 18:00 (UTC) is *coastal,* and the sea breeze around 20:00 (UTC) is depicted by *sea*. The PCASP detects particles from 143 nm to three microns. The size distributions are dominated by small aerosols, especially less than 0.4 microns during all wind conditions. There is a slight dip in the land breeze size distribution around 0.25 microns, due to a temporary failure of the probe. The land breeze has the largest concentration of particles in the mid-size (0.3–0.7 microns) range, while the coastal period has the highest concentration of particles larger than 1.3 micron. This is consistent with the Angstrom coefficient data obtained from the NEPH measurements. The sea breeze periods contain the lowest concentration of

particles across the PCASP range, which is consistent with the overall lower NEPH measurements.

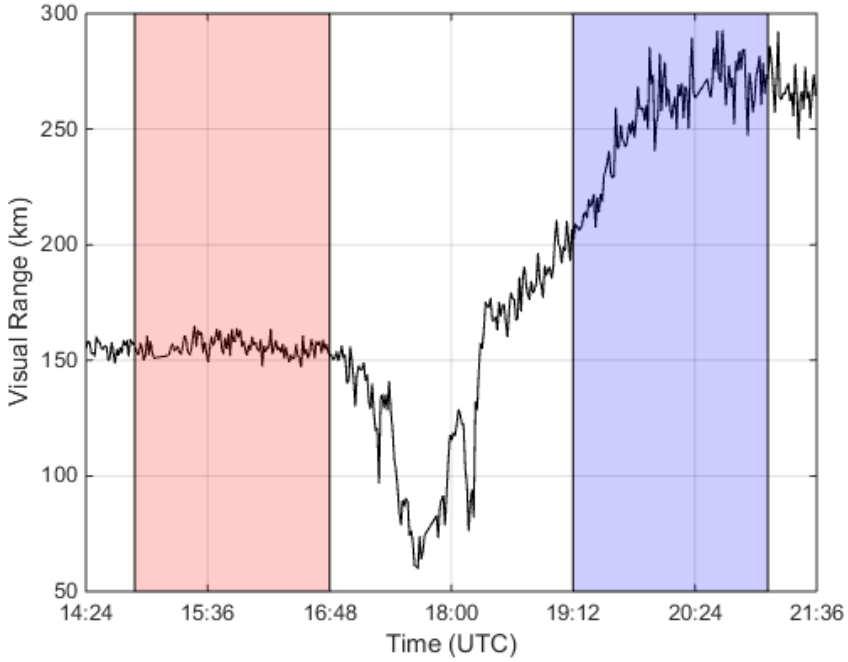

Red shading on the plot indicates land breeze while the blue shading indicates sea breeze. Unshaded sections indicate either light and variable winds or coastal-parallel winds.

Figure 20. Visual Range Derived from NEPH TS on 14 October 2015.

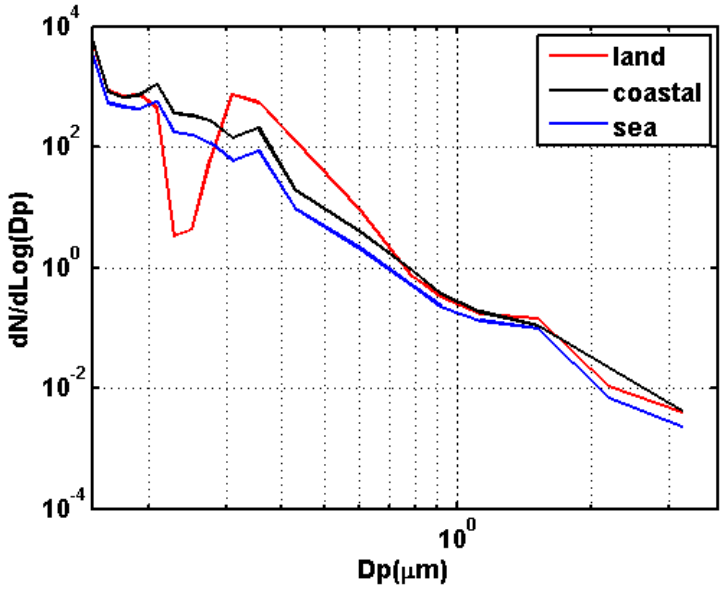

Figure 21. Aerosol Size Distribution in Different Wind Conditions on 14 October 2015.

Another time series where the winds start as a land breeze, shifts to a sea breeze for a short period, and then returns to a land breeze is shown in Figure 22. The wind speed remains relatively constant at 3–4 ms^{-1}. This case provides an in-depth comparison of the land and sea breeze conditions with small contributions from the surf zone. The CPC counts were scaled by a factor of 200 to provide data of the same range as the scattering coefficients. In this case, the land breeze has a TS coefficient from the NEPH that is 2.5 times larger than those during sea breeze. The CPC detections continue to show that the land breeze contains higher particle concentrations than the sea breeze. The NEPH TS was converted to visual range using Equation (4), and is shown in Figure 23.

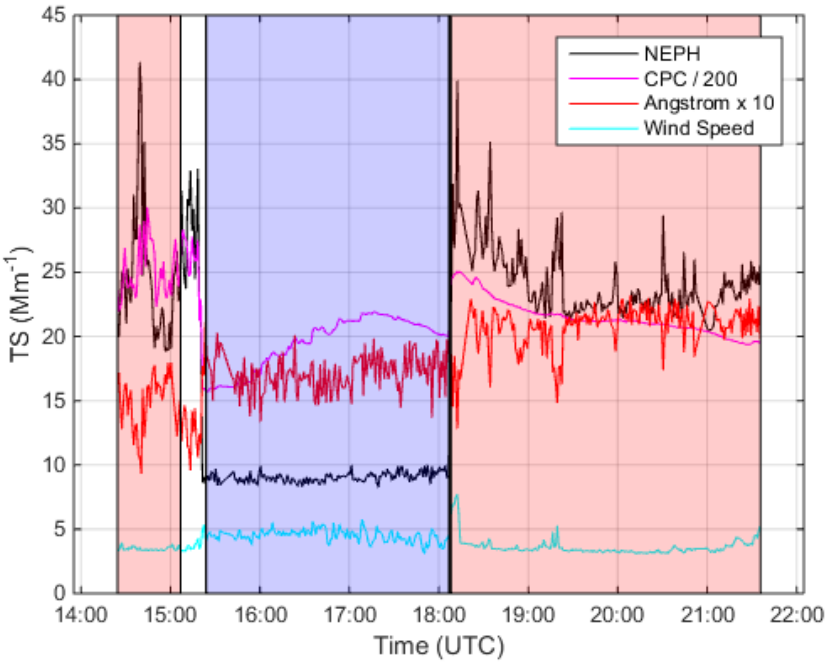

Red shading on the plot indicates land breeze while the blue shading indicates sea breeze. Unshaded sections indicate either light and variable winds or coastal-parallel winds.

Figure 22. Pier-Based Aerosol and Scattering/Extinction Measurements in Periods of Different Wind Directions on Pier Data on 16 October 2015.

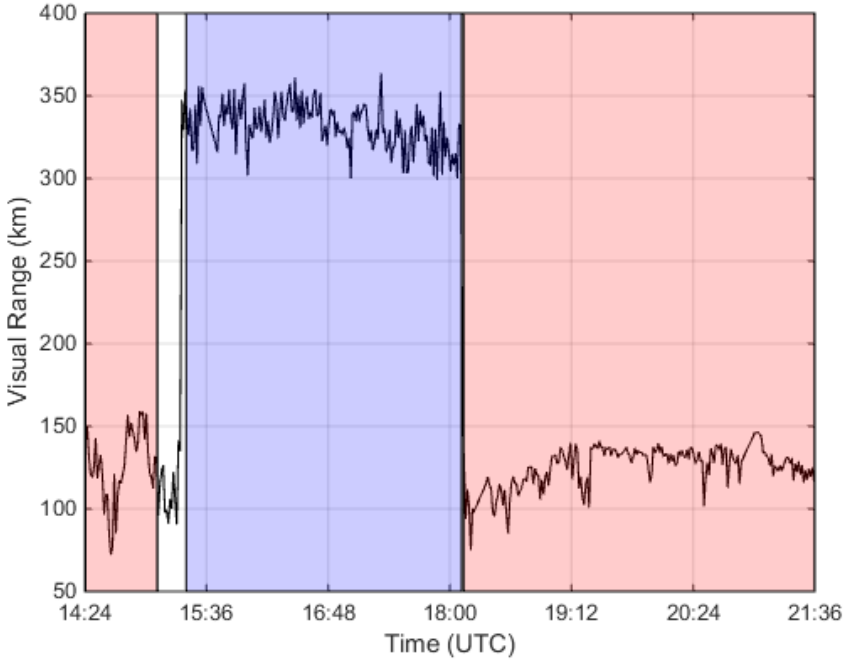

Red shading on the plot indicates land breeze while the blue shading indicates sea breeze. Unshaded sections indicate either light and variable winds or coastal-parallel winds.

Figure 23. Visual Range Derived from NEPH TS on 16 October 2015.

The size distributions for the previously examined period are shown in Figure 24. *Land1* represents the land breeze period at 15:00 (UTC), *sea* depicts the sea breeze period at 16:30 (UTC), and *land2* depicts the land breeze period at 20:00 (UTC). Both periods of land breeze have higher concentrations of optically active particles than the sea breeze period. Above two microns however, the sea breeze size distributions show a relative increase in particle concentration to where the large particles match the land breeze cases. Clearly, the difference in extinction in this case is due to higher concentration of small particles less than two microns in diameter during the land breeze periods.

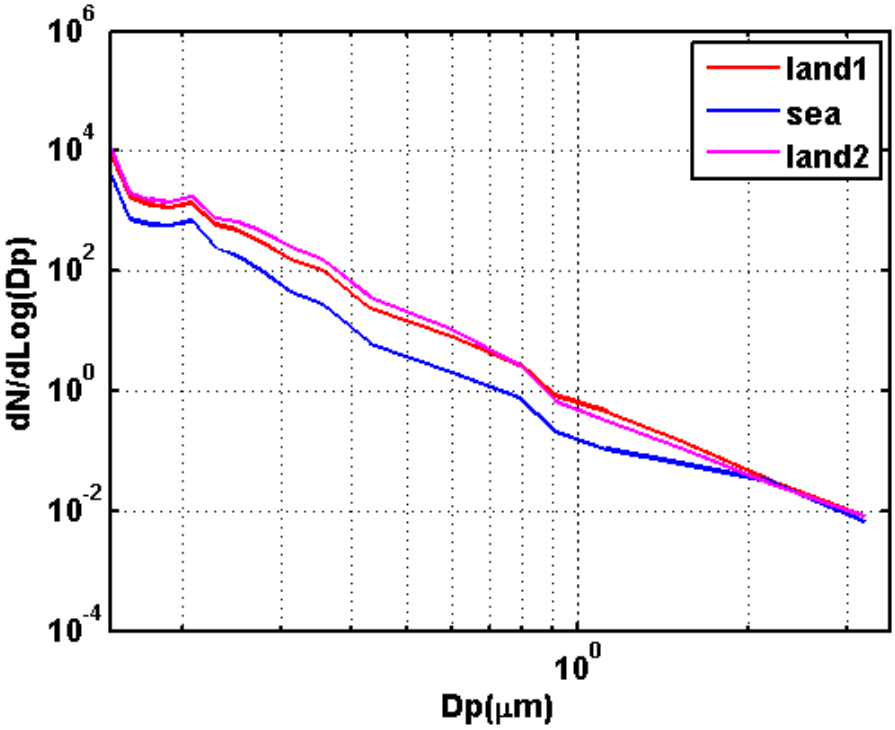

Figure 24. Aerosol Size Distribution in Different Wind Conditions on 16 October 2015.

E. AIRCRAFT DATA

The CIRPAS Twin Otter operated on 11 days during the experiment and flew along preplanned tracks. One of the main instruments used was PCASP which measured aerosol particle size distribution. This was used to examine variability in the aerosol over the ocean. Only two of the 11 flights showed significant variations in the aerosol and are examined further.

The altitude of a typical aircraft (AC) flight is shown in Figure 25. The Twin Otter would initially fly through the various layers of the atmosphere to obtain vertical atmospheric sounding profiles. The Twin Otter periodically flew at very low levels for a short period of time for near-surface sampling of the environment, before settling on long leg mid-level (300 meters) passes that would start in open ocean and travel toward the shore line, before turning around to repeat the process as well as long legs traveling north and south paralleling the coastline. These long legs at constant altitude were in support of

the CTV operation, but the Twin Otter measurements along these legs provide the spatial variability of aerosol content and their radiative effects. All of the aircraft runs took place during the day from 08:00 (UTC) to no later than 19:00 (UTC). The flights performed similar sounding measurements and long leg mid-altitude CTV runs, with slight variances in flight times, and altitude variations.

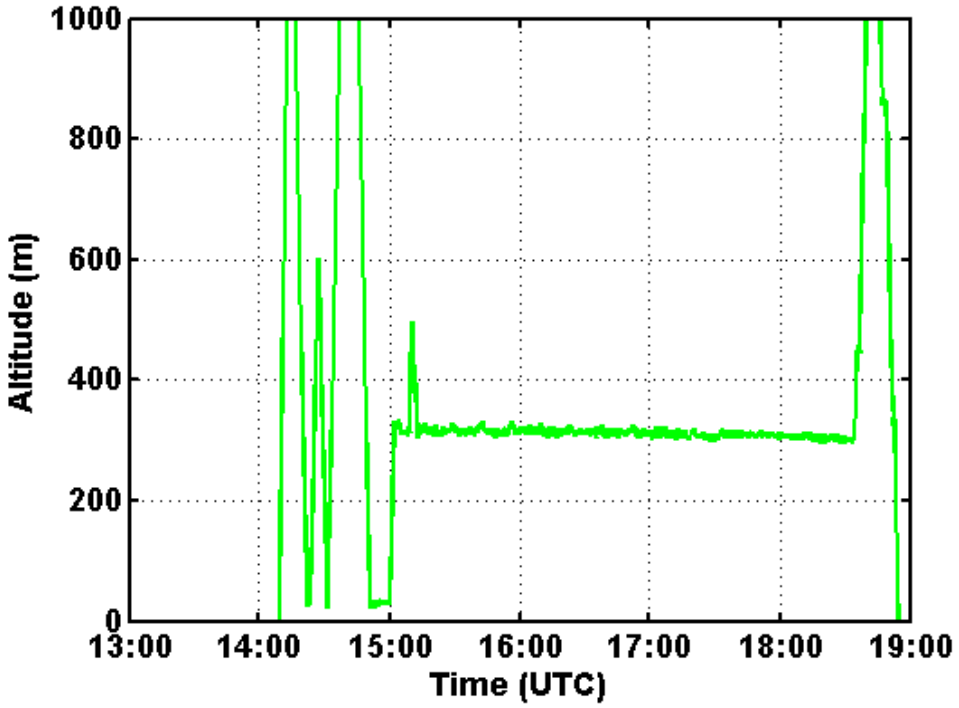

Figure 25. Altitude Data on 17 October 2015.

The aircraft track for 17 October 2015 is shown in Figure 26. The Twin Otter took off from Dare County Regional Airport (MQI) and proceeded to a parallel track along the FRF Pier. Several runs were conducted along this parallel route, including at low level (30 m) and mid-levels (300 m) and then proceeded to a perpendicular track to the FRF Pier, paralleling the coastline. Most of the other aircraft flights for CASPER were similar in route.

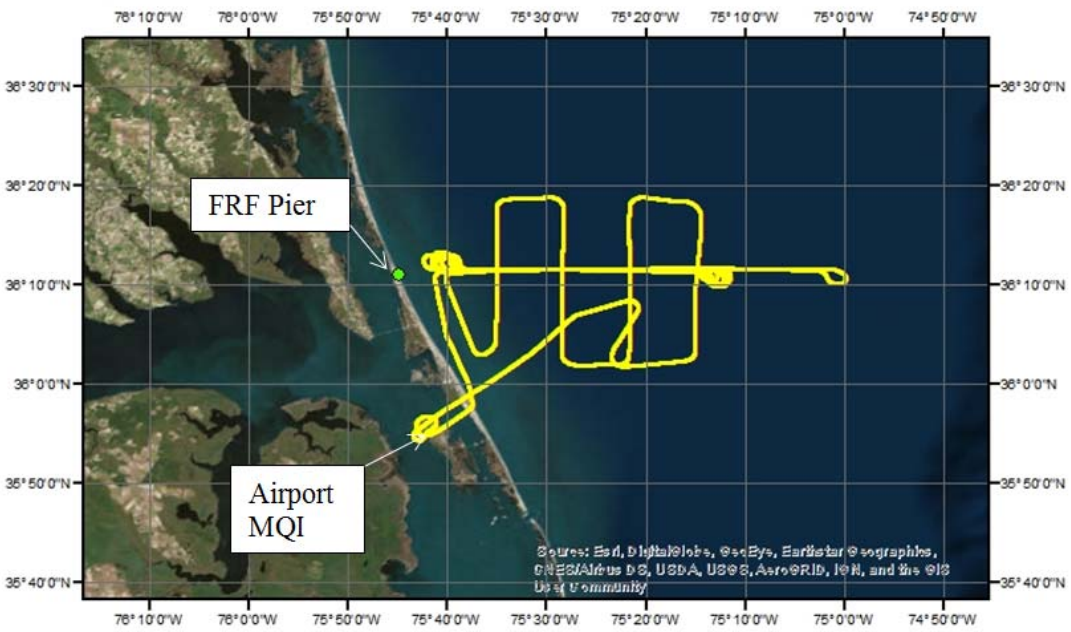

Figure 26. Twin Otter Flight Path on 17 October 2015.

The PCASP size distribution from each run was converted to total scatter, (explained in IV.A.3. PCASP Conversion to Scattering section) and plotted. Data from five straight legs away from the coast, five legs towards the coast, as well as data from the periods where the aircraft is turning around is shown in Figure 27. The aircraft track of the data is shown in Figure 28. As the SST fluctuates between 19 and 20.5^{o}C, the total scatter behaves as the inverse. At the high SST of 20.5, the total scatter is near a minimum around 8 Mm^{-1}. When the SST is at a minimum of 19^{o}C, TS is at a maximum around 14 Mm^{-1}. One also notices the two distinct peaks during the maximum TS period. The wind was from the north at 6 ms^{-1} and the air temperature at 300 m altitude was 15^{o}C, indicating considerable instability when compared with the sea surface temperature and that cold air was advecting into the area.

The peak in total scatter appears coincidental with a transition zone in the ocean temperature (front) with lower scattering on both sides. However, over the colder water near the coast, where instability and convective mixing are less, the scattering coefficient remains higher than over the warmer water further out to sea. Isolating a straight leg, shown in Figure 29, shows this as well.

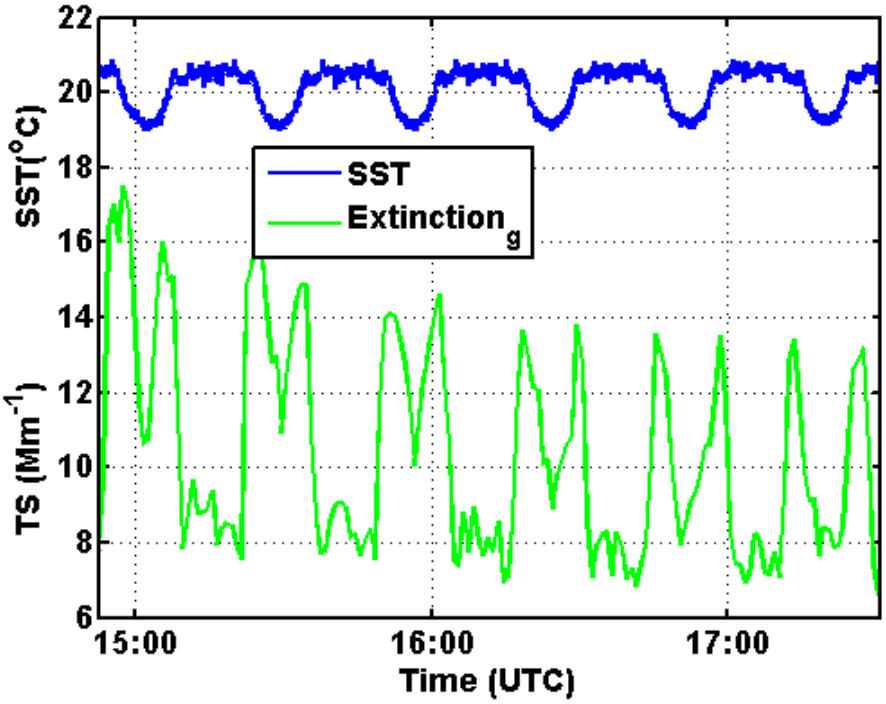

Figure 27. Aircraft PCASP and SST Comparison on 17 October 2015.

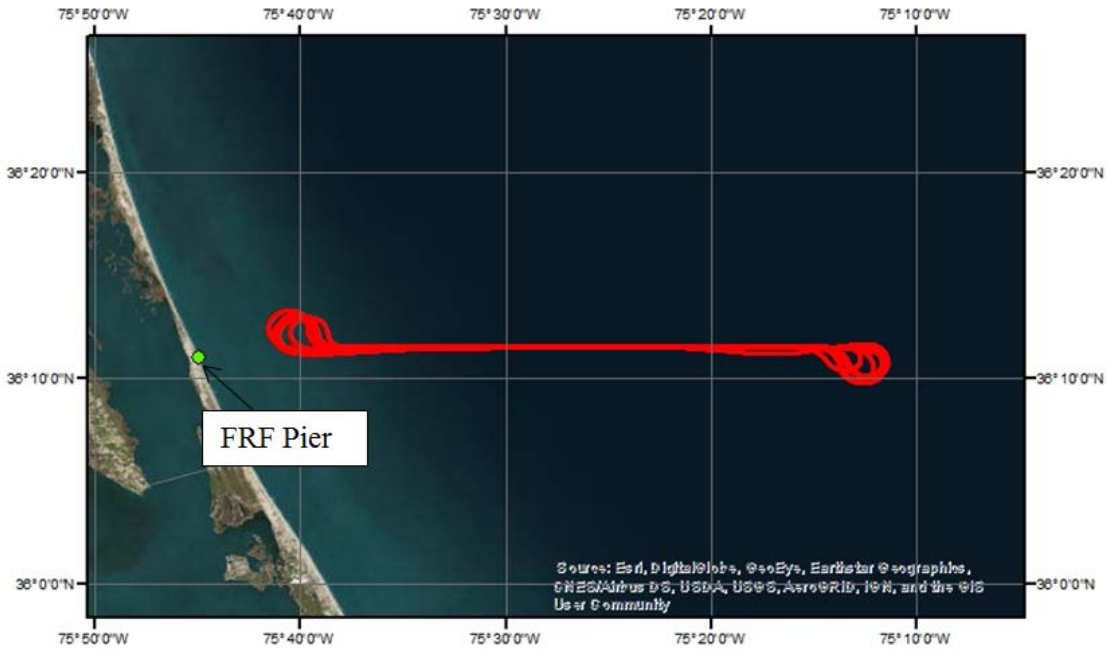

Figure 28. Twin Otter Cross-Coast Flight Path on 17 October 2015.

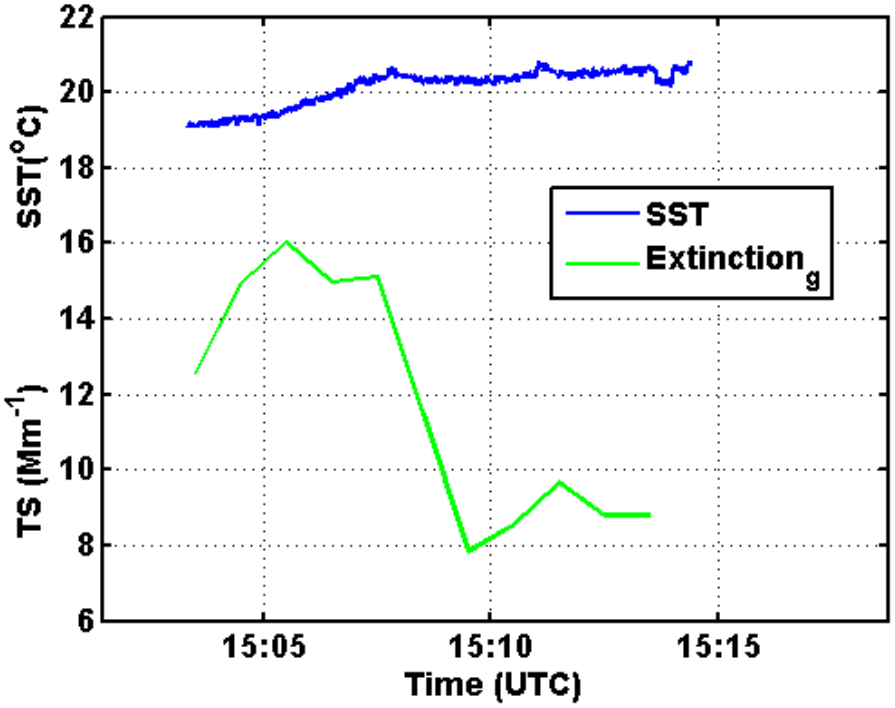

Figure 29. SST and Total Scattering Measurements from a Level-Leg Away from the Coast on 17 October 2015.

Extinction for all five tracks is shown in Figure 30 as a function of distance from the coast. All of the tracks show a maximum above the ocean front where the warmer water meets the cooler coastal water.

The corresponding visual range for these five legs is shown in Figure 31, indicating a factor of two change in visual range in the air above warm water versus that over the cooler water closer to the coast.

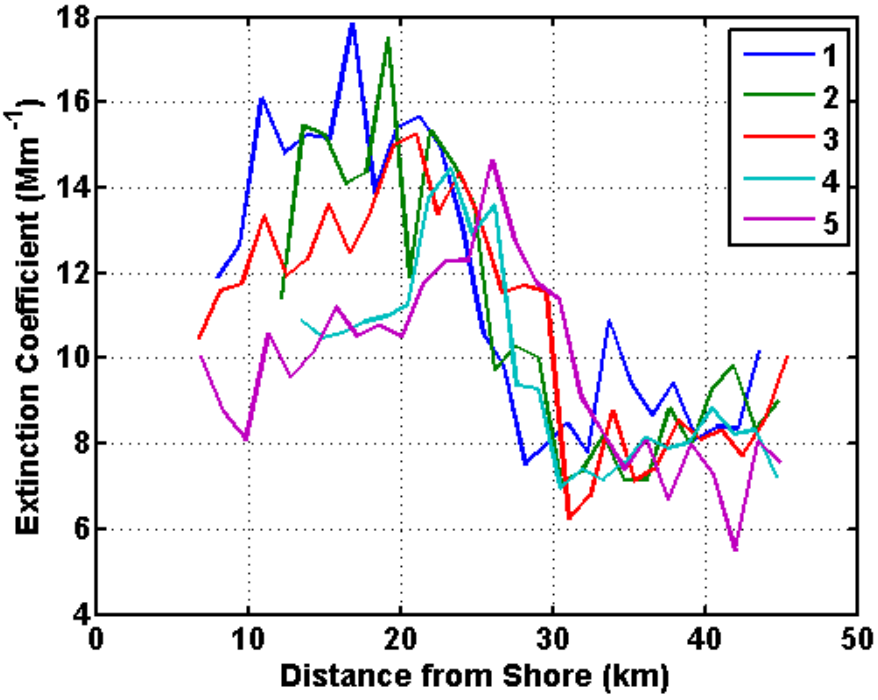

Figure 30. Multiple Level-Leg Measurements Away from the Coast on 17 October 2015.

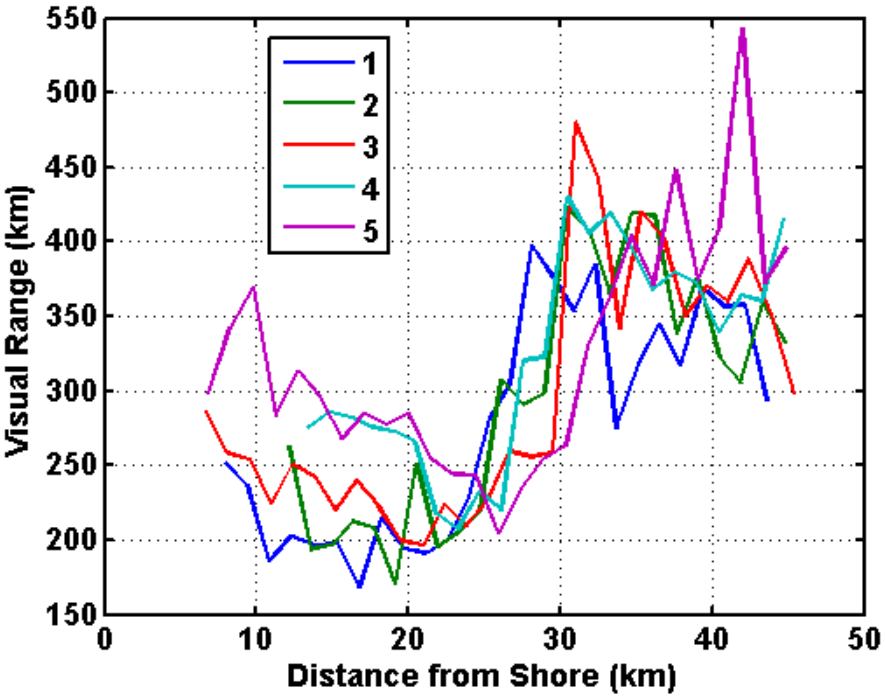

Figure 31. Derived Visual Range from Multiple Level-Leg Measurements Away from the Coast on 17 October 2015.

On 30 and 31 October 2015, the aircraft collected data over the Gulf Steam. The flight path from 31 October 2015 is shown in Figure 32. The flight path from 30 October 2015 was very similar to 31 October 2015. On 30 October, the winds were northeasterly and 10 ms^{-1}, and became north or northwesterly at 3–5 ms^{-1} by 31 October 2015. The aircraft flew at an altitude of 300 m, repeatedly crossing the Gulf Stream front, where the SST gradient was even stronger than in the case on 17 October 2015. In the northeasterly flow on 30 October, no variation was seen in the aerosol as the airplane crossed the Gulf Stream, but on 31 October, a sharp aerosol front appeared at the Gulf Stream edge.

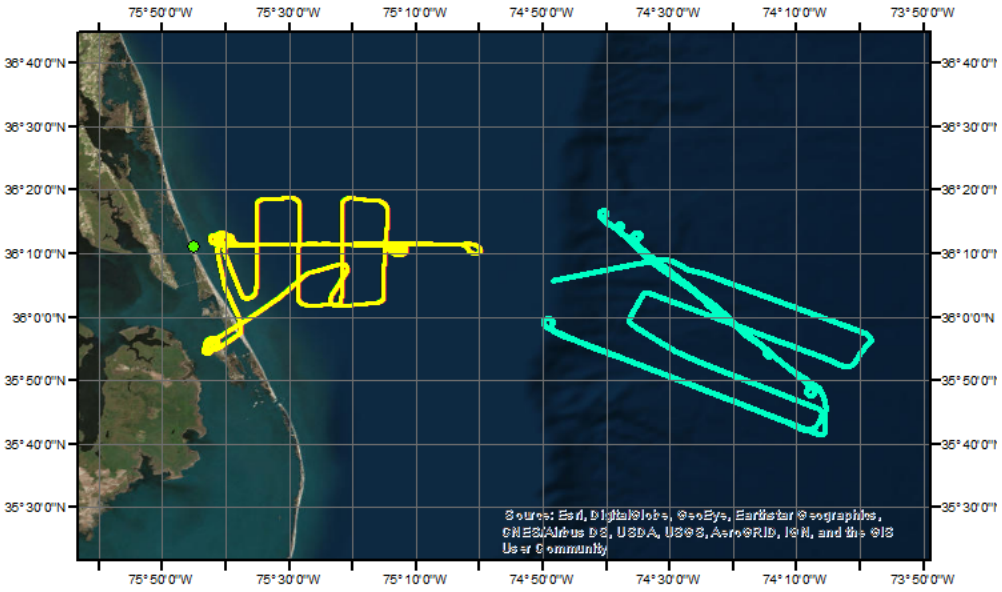

17 October 2015 flight track is shown in yellow and the 31 October 2015 flight track is shown in turquoise for reference.

Figure 32. Twin Otter Flight Paths on 17 and 31 October 2015.

Figure 33 shows a time trace of the extinction coefficient and SST when the aircraft crossed the Gulf Stream front. Over the cold waters closer to the coast, the extinction is over twice as large as over the warmer Gulf Stream waters. As on 17 October 2015, the air temperature at 300 m was 15°C, or 5°C colder than the SST in the colder water, and as much as 10°C colder than that of the warmer water. Clearly, cold air was advecting in the area. The sounding showed a well-mixed boundary layer to 600 m

height on both days. A marked discontinuity in the aerosol, coincidental with the Gulf Stream front, with 50 to 100 percent larger extinction coefficients occurred over the colder coastal waters than over the warmer Gulf Stream.

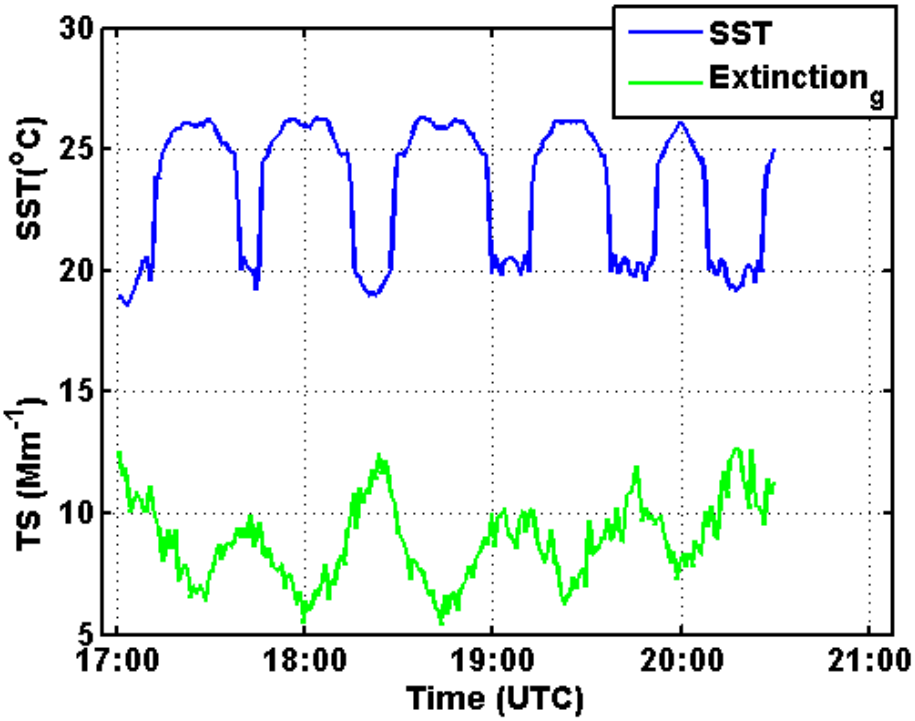

Figure 33. Total Extinction Derived from Aircraft PCASP Measurements and Corresponding SST on 31 October 2015.

V. SUMMARY AND CONCLUSIONS

A. DISCUSSION

Accurate prediction and depiction of the environment, including sea salt aerosols, is critical in quantifying effects of the atmosphere on electromagnetic wave propagation; however, there is a lack of data adequate for model evaluation or improvement. The marine boundary layers, especially near the coastal regions, are characteristically heterogeneous and often transient and the ocean and atmosphere surface layer dynamics need to be understood and adequately represented in surface-flux parameterizations as well as in evaporative duct prediction models.

CASPER-East was designed to address knowledge gaps related to EM wave propagation in the coastal MABL with an ultimate objective of "fully characterizing the MABL as an EM propagation environment" (Wang et al. 2015). The data collected during CASPER-East were analyzed to determine the aerosol characteristics, specifically absorption and total scatter coefficients. This provides an important dataset that can be used to improve and tune aerosol and visibility prediction models to forecast targeting and detection ranges. Future developments in improving propagation prediction depend on understanding the atmosphere and upper ocean interactions, and correctly quantifying the characteristics of the surface layer environment. This thesis work attempts to quantify surface zone-generated aerosols with persistent measurements over a period of one month.

Offshore to onshore breeze transition periods were examined and total scatter from the NEPH closely followed the trend of the particle concentrations measured by the CPC. Although the sea breeze may contain larger sized particles than the land breeze, the small and more numerous land-sourced particles often are sufficient to dominate the optical effects over the fewer and larger sea-sourced particles.

No close correlation is observed between the aerosol extinction at Duck, North Carolina and the wind direction, except in cases when winds are along the coast. This may be due to the geographical conditions at Duck, North Carolina. A large body of

water is not only on the Atlantic side of the site, but also a short distance to the west. Thus, surf generation of particles is possible in both land and sea breezes.

Particle concentrations show some dependence on wind speed. During sea breeze periods with wind speeds greater than 8 ms^{-1}, significantly lower concentrations are observed than during land breeze periods with similar wind speeds. During frequently shifting winds, a halo of land sourced aerosol may be formed some distance off the coast, which swings back to shore when wind shifts to a sea breeze. At low wind speeds this may continue until the wind shifts again, while at higher speed, chances are that pristine marine aerosol may reach the shores.

In sustained along-shore wind periods with an active surf zone, a large impact is observed on the optical effects of the aerosol. In such cases, the fetch allows increased aerosol flux into the atmosphere due to the long distances along the air parcel trajectory over the surf zone, and the coastal aerosol reaches steady state. In cross-shore flows, the surf zone affecting the coastal site is smaller than the fetch area around the coastal site and the aerosol concentration probably does not reach equilibrium state. Visual range dropped by an order of magnitude during such an episode compared with prior land breeze and subsequent sea breeze. In very strong winds however, with a very active ocean filled with whitecaps, the effect of particle generation in the surf zone probably matters little, and the aerosol extinction probably is equally powerful with on-shore winds.

Particle size distributions show that during land breezes, the mid-size aerosol (sub-micron) dominates the particle concentration, while during sea breezes concentration of coarse mode particles (super-micron) is enhanced. Although the coarse mode weighs much more in extinction calculations, often the larger number of mid-size particles is sufficient to dominate the optical effects.

In low on-shore wind periods, with no surf at the coast, the visual range is observed to improve by factors of 3–4 with the marine air over the land breeze air. Again this is due to much more numerous mid-sized particles in the land breeze, and absence of coarse mode particles in the calm sea breeze.

The aircraft data show that there is a strong transport barrier associated with sharp sea surface temperature gradients in unstable air during cold advection of land- and surf-contaminated aerosol. This is attributed to enhanced convective mixing over warmer waters. The convection raises the boundary layer height and mixes the surface-sourced aerosol to higher altitudes. This has dramatic effects on particle concentration at the lower levels. Visual range deteriorated by a factor of two at 300 m altitude crossing the Gulf Stream ocean front, where the SST changed abruptly by 6^{o}C. On a flight where the wind direction was more northeasterly, and cold marine air advected into the area, no effect on optical properties was detected.

B. FUTURE WORK

Future work should continue to focus on collecting data in the MABL that is adequate for model evaluation or improvement. Accurate prediction and depiction of the environment is critical in quantifying effects of the atmosphere on electromagnetic wave propagation. Further analysis could be conducted to determine the surf-sourced extinction and visual range modulation and then analyzed for dependence on wind and sea state. This dataset should also be used in optical propagation models to see the impact on high energy lasers (HEL).

Since CASPER-East was designed for ducting research, future experiments could be designed specifically for examination of coastal aerosols. The aircraft flight path could be extended over the coastline and land mass. This would provide accurate representation of open ocean and pure continental aerosols. Also, Duck, North Carolina was not ideal, as there is only a narrow land mass surrounded by water. This prevented experimental data from being collected on pure land aerosols, and instead provided a water mass that contributed aerosols to the associated land breeze. Also, the prevailing westerlies flood the experiment site with continental atmosphere. The west coast would be an ideal location for examining marine aerosol.

THIS PAGE INTENTIONALLY LEFT BLANK

LIST OF REFERENCES

Anderson, T. L., and J. A. Ogren, 1998: Determining aerosol radiative properties using the TSI 3563 Integrating Nephelometer. *Aerosol Sci. and Tech.*, **29**, 57–69. doi:10.1080/02786829808965551.

Baumgardner, D., 2005: Passive cavity aerosol spectrometer probe. Earth System Research Laboratory, Accessed 10 October 2016. [Available online at http://esrl.noaa.gov/gmd/aero/instrumentation/pcasp100.html.]

Bennett, A., 2012: Introduction to atmospheric visibility estimation. Biral, Accessed 21 May 2017. [Available online at http://www.biral.com/wp-content/uploads/2015/02/Introduction_to_visibility-v2-2.pdf.]

Bond, T. C., T. L. Anderson, and D. Campbell, 1999: Calibration and intercomparison of filter-based measurements of visible light absorption by aerosols. *Aerosol Sci. and Tech.*, **30**, 582–600. doi:10.1080/027868299304435.

Bond, T. C., D. S. Covert, and T. Muller, 2009: Truncation and angular-scattering corrections for absorbing aerosol in the TSI 3563 Nephelometer. *Aerosol Sci. and Tech.*, **43**, 866–871. doi:10.1080/02786820902998373.

Dennis, R., 1976: Introduction: objectives, organization, and applications. *Handbook on Aerosols,* R. Dennis, Ed., Technical Information Center Energy Research and Development Administration, 1–6.

Edson, J., and Coauthors, 1999: *Coupled marine boundary layers and air-sea interaction initiative combining process studies, simulations and numerical models.* Office of Naval Research, 144 pp.

Fenn, R. W., 1976: Optical properties of aerosols. *Handbook on Aerosols,* R. Dennis, Ed., Technical Information Center Energy Research and Development Administration, 66–92.

Gallaudet, T., 2016: Naval Oceanography Electromagnetic Maneuver Warfare Strategy. *Naval Meteorology and Oceanography Command*, 1–6.

Hale, R., T. Wendt, W. Nuss, and Q. Wang, 2016: *Synoptic summary coupled air-sea processes and electromagnetic ducting research – East Coast Campaign.* Dept. of Meteorology, Naval Postgraduate School, 53 pp.

Hess, M., P. Koepke, and I. Schult, 1998: Optical properties of aerosols and clouds. *Bulletin of the American Meteorological Society,* **79**, 831–844. doi:10.1175/1520-0477.

Levoni, C., M. Cervino, R. Guzzi, and F. Torricella, 1997: Atmospheric aerosol optical properties: a database of radiative characteristics for different components and classes. *Applied Optics*, **36**, 8031–8041. doi:0003-6936/97/308031-11.

Lewis, E. R., 2004: *Sea salt aerosol production: mechanisms, methods, measurements and models – a critical review.* American Geophysical Union, 413 pp.

Naval Meteorology and Oceanography Professional Development Detachment Atlantic, 2005: Atmospheric effects on EO sensors and systems. United States Navy, Accessed 3 May 2017. [Available online at http://www.deltagearinc.com/library/OpticsFacts/EO.pdf.]

Naval Meteorology and Oceanography Command Public Affairs, 2016: Naval Oceanography releases Electromagnetic Maneuver Warfare Strategy. United States Navy, Accessed 24 March 2016. [Available online at http://www.navy.mil/submit/display.asp?story_id=93788.]

Resch, F., 1986: Oceanic air bubbles as generators of marine aerosols. *Oceanic Whitecaps and Their Role in Air-Sea Exchange Processes,* E. C. Monahan and G. M. Niocaill, Eds., D. Reidel Publishing Company, 101–112.

Spiel, D. E., and G. D. Leeuw, 1996: Formation and production of sea spray aerosol. *Journal of Aerosol Sci.,* **27**, S65–S66, doi:0021-8502/96.

Stewart, K. A., 2014: NPS Meteorology examines effects on electromagnetic waves. CHIPS, Department of the Navy, Accessed 9 February 2017. [Available online at http://www.doncio.navy.mil/CHIPS/ArticleDetails.aspx?ID=5526.]

TSI Incorporated, 2006: Condensation Particle Counter Model 3010. Accessed 10 October 2016. [Available online at http://www.tsi.com/condensation-particle-counter-3010/.]

TSI Incorporated, 2012: Integrating Nephelometer 3563. Accessed 10 October 2016. [Available online at www.tsi.com/integrating-nephelometer-3563/.]

Twomey, S., 1977: *Atmospheric aerosols*. Elsevier Scientific Publishing Company, 302 pp.

University Corporation for Atmospheric Research (UCAR), 2014: Introduction to electromagnetic and electro-optical propagation. Accessed 3 May 2017. [Available online at https://www.meted.ucar.edu/oceans/emeo/index.htm.]

Virkkula, A., 2010: Correction of the calibration of the 3-wavelength particle soot absorption photometer (3 λ PSAP). *Aerosol Sci. and Tech.*, **44**, 706–712. doi:10.1080/02786826.2010.482110.

Virkkula, A., N. C. Ahlquist, D. S. Covert, W. P. Arnott, P. J. Sheridan, P. K. Quinn, and D. J. Coffman, 2005: Modification, calibration and a field test of an instrument for measuring light absorption by particles. *Aerosol Sci. and Tech.*, **39**, 68–83. doi:10.1080/027868290901963.

Wang, Q., R. Burkholder, J. Fernando, D. Khelif, R. K. Shearman, and L. Shen, 2015: CASPER – a new multidisciplinary research initiative on electromagnetic wave propagation in the marine atmosphere. *2015 USNC-URSI Radio Science Meeting (Joint with AP-S Symposium), USNC-URSI 2015 – Proceedings*, Vancouver, Canada, Institute of Electrical and Electronics Engineers Inc., 252. doi:10.1109/USNC-URSI.2015.7303536.

Wang, Q., and Coauthors, 2017: CASPER: Coupled Air-Sea Processes and Electromagnetic (EM) Wave ducting Research. Submitted for Publication in the *Bulletin of America Meteorological Society*, 48 pp.

THIS PAGE INTENTIONALLY LEFT BLANK

INITIAL DISTRIBUTION LIST

1. Defense Technical Information Center
   Ft. Belvoir, Virginia

2. Dudley Knox Library
   Naval Postgraduate School
   Monterey, California